NASA Technical Memorandum 74056

Static Aerodynamic Characteristics of a Single-Stage-to-Orbit Vehicle With Low Planform Loading at Mach Numbers From 0.3 to 4.63

Delma C. Freeman, Jr., and Roger H. Fournier

NOVEMBER 1977

NASA

NASA Technical Memorandum 74056

Static Aerodynamic Characteristics of a Single-Stage-to-Orbit Vehicle With Low Planform Loading at Mach Numbers From 0.3 to 4.63

Delma C. Freeman, Jr., and Roger H. Fournier
Langley Research Center
Hampton, Virginia

National Aeronautics
and Space Administration

**Scientific and Technical
Information Office**

1977

SUMMARY

An investigation was conducted in the Langley 8-foot transonic pressure tunnel and in the Langley Unitary Plan wind tunnel to determine the longitudinal and lateral aerodynamic characteristics of a single-stage-to-orbit vehicle. The vehicle utilized an all metallic, hot structure, thermal protection system which resulted in low planform loading. The model was tested over a Mach number range from 0.3 to 4.63 for an angle-of-attack range from -4° to 32° at both 0° and 5° sideslip. Tests were made to determine the static longitudinal stability and trim, the static lateral-directional stability, and the base pressures of the model.

The results of the investigation show that the model was longitudinally unstable at the lowest Mach number (M = 0.3), but as the Mach number approached transonic conditions, the model became longitudinally stable. For the supersonic Mach numbers, the stability level decreased, and at the higher Mach numbers (M = 3.95 and 4.63), the model was either neutrally stable or slightly unstable. The model required only small elevon deflections to trim, except at Mach numbers of 1.2 and 2.86 where large negative deflections were required. The model was directionally stable throughout the angle-of-attack range at subsonic and transonic speeds, but at Mach 2.36 the model became unstable at 8° angle of attack. At the highest Mach numbers, the model was directionally unstable even at the low angles of attack.

INTRODUCTION

The Space Shuttle Program is now in the final development stages and hardware is being fabricated. Current studies indicate that a follow-on, Earth-orbital transportation system could be required around 1995, if the new system can offer significant cost/performance advantages over the system in use at that time. Based upon these projections, study of advanced transportation systems is continuing within the National Aeronautics and Space Administration. (See ref. 1.)

One concept that has evolved as a possible design approach is a single-stage-to-orbit, sled-launched vehicle with an all metallic, hot structure, thermal protection system. In this design, the primary structure serves as both propellant tankage and thermal protection system.

The unique design features of assisted horizontal takeoff and hot structure during entry require low planform loading and large, vehicle planform area.

A model of this design was tested in wind tunnels at Langley Research Center to determine the static longitudinal stability and trim, the static lateral-directional stability, and the base pressures of the model. The tests were conducted over the subsonic, transonic, and supersonic Mach number ranges

for angles of attack from -4° to 32°. The results of the tests are presented and discussed.

SYMBOLS

The longitudinal data are referred to the stability axis system, and the lateral-directional data are referred to the body axis system. (See fig. 1.) The moment center was located at 71 percent of the body length from nose (indicated in fig. 2).

b reference wing span, 42.56 cm

C_D drag coefficient, $\frac{\text{Drag}}{qS}$

C_L lift coefficient, $\frac{\text{Lift}}{qS}$

C_l rolling-moment coefficient, M_X/qSb

C_{l_β} $= \frac{\Delta C_l}{\Delta \beta}$, $\beta = 0^\circ$ and 5°

C_m pitching-moment coefficient, $M_Y/qS\bar{c}$

C_n yawing-moment coefficient, M_Z/qSb

C_{n_β} $= \frac{\Delta C_n}{\Delta \beta}$, $\beta = 0^\circ$ and 5°

C_p base-pressure coefficient

C_Y side-force coefficient, $\frac{\text{Side force}}{qS}$

C_{Y_β} $= \frac{\Delta C_Y}{\Delta \beta}$, $\beta = 0^\circ$ and 25°

c wing section chord

$\bar{c}$ mean aerodynamic chord, 24.89 cm

D drag, N

F_Y side force, N

L lift, N

l body length, cm

M Mach number

M_X rolling moment, m-N

M_Y pitching moment, m-N

M_Z yawing moment, m-N

q dynamic pressure, Pa

S reference wing area, cm^2

X,Y,Z body reference axes

y distance from vehicle center line

α angle of attack, deg

β angle of sideslip, deg

δ_e elevon deflections, positive when trailing edge is down, deg

δ_r rudder deflection, deg

Subscript:

s stability axis system

MODEL AND APPARATUS

A drawing of the 0.01-scale model used in the investigation (presented in fig. 2) shows a distinct wing-body design having elevon surfaces on the wing and an aft, vertical tail with a rudder. The nonsymmetrical wing section was approximately 10 percent thick at root and tip. The sections are defined by coordinates in tables I and II.

The experimental results were obtained in the Langley 8-foot transonic pressure tunnel and in the Langley Unitary Plan wind tunnel. Data were obtained for Mach numbers from 0.3 to 1.2 in the 8-foot tunnel and from 2.36 to 4.63 in the Unitary Plan tunnel. Operating characteristics of both wind tunnels are presented in reference 2.

TESTS

Static force tests were conducted to determine the longitudinal stability, lateral-directional stability, and base pressure of the model for Mach numbers from 0.3 to 4.63. For the subsonic and transonic Mach numbers (0.3 to 1.2), the model was tested at angles of attack from approximately -2° to 21°, and for the supersonic tests (M = 2.36 to 4.63), the angle-of-attack range was from approximately -4° to 32°. The static, lateral-directional stability characteristics were determined from incremental differences in C_n, C_l, and C_Y measured at 0° and 5° angles of sideslip. The test condiditons were as follows:

Mach number	Dynamic pressure, Pa	Stagnation temperature, K	Reynolds number
0.3	5.98	---	3.81×10^6
.6	20.01	---	6.58
.9	34.04	---	8.21
1.2	21.11	---	4.35
2.36	21.45	339	4.13
2.86	18.91	339	4.13
3.95	14.22	353	4.13
4.63	11.16	353	4.13

For all tests, boundary-layer transition strips (0.16 cm wide) of sparsely distributed carborundum grains were applied to the model 1.27 cm downstream from the leading edge of all lifting surfaces and 3.05 cm aft of the nose. Two sizes of carborundum grains (determined by the methods of ref. 3) were used in the tests: No. 120 at subsonic and transonic Mach numbers (0.3 to 1.2) and No. 45 at supersonic Mach numbers (2.36 to 4.63).

All data have been corrected for sting bending. Drag data include the base pressure.

RESULTS AND DISCUSSION

Static Longitudinal Characteristics

Static longitudinal stability and trim characteristics were plotted for Mach numbers of 0.3, 0.6, 0.9, 1.2, 2.36, 2.86, 3.95, and 4.63 (figs. 3 to 10, respectively). Summary plots of various parameters as functions of Mach number are also presented (figs. 11 and 12).

Longitudinal characteristics.- The static longitudinal stability characteristics C_m/C_L of the model with zero elevon deflection were plotted against Mach number (fig. 11(a)) for 0°, 10°, 20°, and 30° angles of attack. These results show that the model was longitudinally unstable at the lowest Mach number (M = 0.3). As the Mach number approached transonic conditions, the model became longitudinally stable due to the rearward shift of the aerodynamic center.

The reason for the distinct variation of C_m/C_L with Mach number at 20° angle of attack can be seen by comparing figures 5(e) and 6(e). At Mach 1.2, the variation of pitching moment with lift became nonlinear and caused the large variation of C_m/C_L as the Mach number increased from 0.9 to 1.2. For supersonic Mach numbers, the stability level was dependent upon angle of attack. For 0°, 10°, and 20° angles of attack, the model became either neutrally stable or slightly unstable at Mach numbers greater than 3; however, for $\alpha = 30^\circ$ the model was stable throughout the supersonic speed regime. Except at $\alpha = 20^\circ$ and Mach 1.2, the model with zero elevon deflections had linear variations of the pitching moment with angle of attack. Variations of the lift-curve slope at various angles of attack are presented as functions of Mach number in figure 11(b). These results show the characteristic increase in C_{L_α} as transonic Mach numbers are approached and a decrease in C_{L_α} with increased supersonic Mach numbers.

Elevon effectiveness and trim characteristics.- The elevon deflections required for trim at various angles of attack (fig. 12(a)) are small (10° to -10°) except at Mach numbers from 1.5 to 2.5. In this range, large negative elevon deflections are required to trim the model at 10° angle of attack.

One interesting point shown in the basic data (fig. 5) that cannot be seen in the summary plots is a nonlinearity in $C_{m_{\delta_e}}$ at Mach 0.9. (The nonlinearity also appears in $C_{L_{\delta_e}}$ and $C_{D_{\delta_e}}$.) As can be seen from the data plot (fig. 5(d)), the elevon deflection of 10° became completely ineffective at angles of attack above 6°. This phenomenon has been seen in other vehicle designs, including the space shuttle orbiter. The nonlinearity in $C_{m_{\delta_e}}$ was caused by flow separation on the aft portion of the wing. With the elevons at 20° deflection, the flow was separated throughout the test range; however, with the elevons deflected 10°, this separation did not occur until the wing was at approximately 6° angle of attack.

The trimmed-lift coefficient and lift-to-drag ratio are presented as functions of Mach number in figures 12(b) and 12(c), respectively. The results show that, with the large wing dictated by the low wing landing required for the horizontal-takeoff and hot-structure concept, the configuration has sufficient trim-lift coefficient for adequately low landing speeds at reasonable angles of attack. The performance data (lift-to-drag ratios) show (fig. 12(c)) that the model has subsonic, trimmed, lift-to-drag ratios of over 7.5.

Base pressures.- The base and cavity pressures measured during the tests are presented (fig. 13) for use in analysis of the data presented. No discussion of these results is included.

Static Lateral-Directional Characteristics

The static lateral-directional characteristics of the model, with and without the vertical tail, show (fig. 14) that the model with the vertical tail

was directionally stable throughout the angle-of-attack range for the subsonic and transonic tests. At a supersonic Mach number of 2.36, the model became unstable at 8° angle of attack, and at the highest Mach numbers, the model was directionally unstable even at the low angles of attack. The directional stability data measured without the vertical tail, compared to the tail-on data, show that the increment in C_{n_β} due to the vertical tail was sufficient to stabilize the model and was linear with angle-of-attack variations for the subsonic and transonic Mach numbers. At the supersonic Mach numbers, the vertical tail became less effective at the higher angles of attack due to the shielding by the wing and body. This made the configuration directionally unstable in the operational angle-of-attack range.

Also measured in the tests, the effective dihedral parameter shows (fig. 14) that the model (tail on) had positive effective dihedral $\left(-C_{l_\beta}\right)$ throughout the angle-of-attack range at Mach numbers up to 2.86. At Mach numbers of 3.95 and 4.63, C_{l_β} was positive at angles of attack near zero but became negative as lift began to develop on the wing at positive angles of attack.

SUMMARY OF RESULTS

An investigation was conducted to determine the subsonic, transonic, and supersonic aerodynamic characteristics of a single-stage-to-orbit vehicle with an all metallic, hot structure, thermal protection system. The results of these tests are summarized as follows:

1. The model was longitudinally unstable at the lowest Mach number (M = 0.3), but as the Mach number approached transonic conditions, the model became longitudinally stable. For the supersonic Mach numbers, the stability level decreased, and at the higher Mach numbers (M = 3.95 and 4.63), the model was either neutrally stable or slightly unstable.

2. The model required only small elevon deflections (-10° to 10°) to trim over the test range, except at Mach numbers of 1.2 and 2.86 where large negative deflections were required to trim. The model exhibited a nonlinearity in the variation of pitching moment with elevon deflection at Mach 0.9.

3. The model with the vertical tail had directional stability throughout the angle-of-attack range (-4° to 32°) at subsonic and transonic speeds, but at Mach 2.36 the model became unstable at 8° angle of attack. At the highest Mach numbers, the model was directionally unstable even at the low angles of attack.

4. The results show that the model (tail on) had positive effective dihedral throughout the test range at Mach numbers up to 2.86. At Mach numbers of 3.95 and 4.63, the effective dihedral was positive at angles of attack near zero but became negative as lift began to develop on the wing at positive angles of attack.

Langley Research Center
National Aeronautics and Space Administration
Hampton, VA 23665
October 12, 1977

REFERENCES

1. Henry, Beverly Z.; and Decker, John P.: Future Earth Orbit Transportation Systems/Technology Implications. Astronaut. & Aeronaut., vol. 14, no. 9, Sept. 1976, pp. 18-28.

2. Schaefer, William T., Jr.: Characteristics of Major Active Wind Tunnels at the Langley Research Center. NASA TM X-1130, 1965.

3. Braslow, Albert L.; Hicks, Raymond M.; and Harris, Roy V., Jr.: Use of Grit-Type Boundary-Layer-Transition Trips on Wind-Tunnel Models. NASA TN D-3579, 1966.

TABLE I.- AIRFOIL-TIP SECTION COORDINATES

Station, percent c	Upper, percent c	Lower, percent c
5.0	0.037	0.0222
7.5	.0407	.0241
10.0	.0444	.0248
20.0	.0593	.0278
30.0	.0685	.0278
40.0	.0722	.0296
50.0	.0704	.0296
60.0	.0611	.0278
70.0	.0573	.0222
80.0	.0389	.0185
90.0	.0241	.0074
100.0	0	0
Leading-edge radius = 0.030c y = 19.685 cm		

TABLE II.- AIRFOIL-ROOT SECTION COORDINATES

Station, percent c	Upper, percent c	Lower, percent c
2.5	0.0266	0.0142
5.0	.039	.0164
7.5	.0496	.0177
10.0	.0567	.019
20.0	.074	.0204
30.0	.082	.0271
40.0	.0828	.0221
50.0	.0797	.0234
60.0	.0118	.0239
70.0	.0589	.0221
80.0	.0421	.0168
90.0	.0235	.0102
Leading-edge radius = 0.012c y = 5.334 cm		

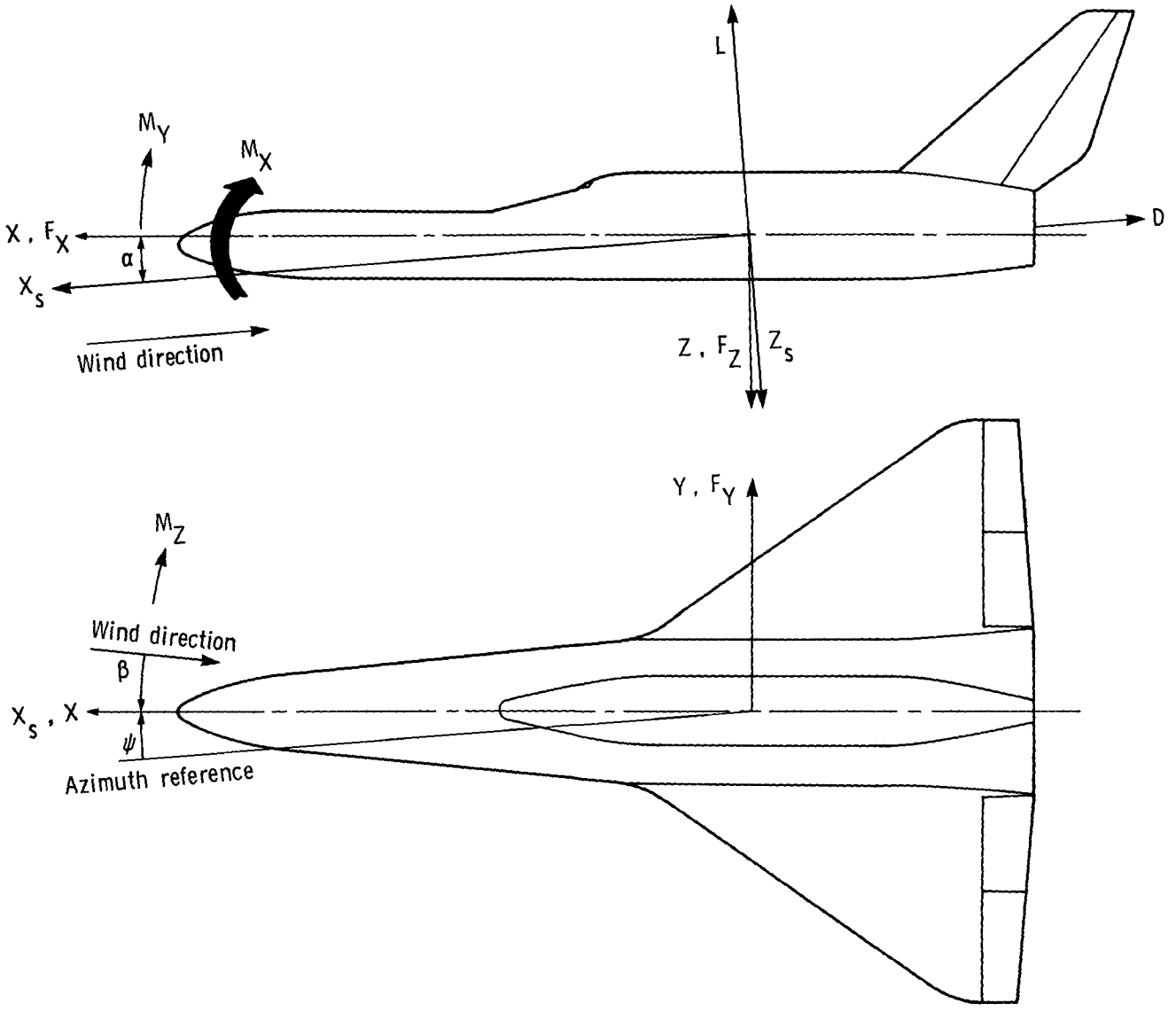

Figure 1.- System of axes used in investigation. Arrows indicate positive direction of moments, forces, and angles.

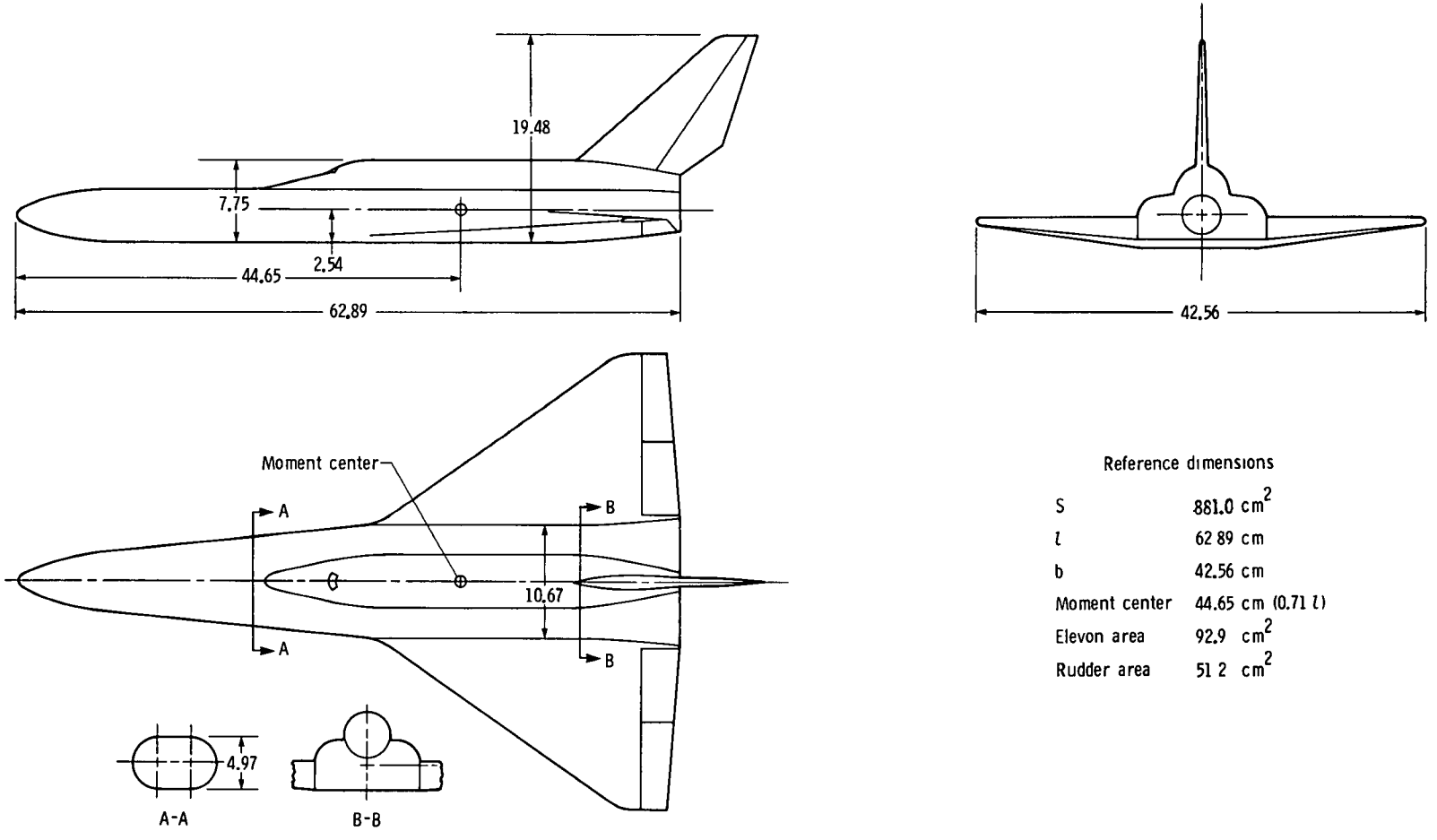

Reference dimensions

S	881.0 cm^2
l	62 89 cm
b	42.56 cm
Moment center	44.65 cm (0.71 l)
Elevon area	92.9 cm^2
Rudder area	51 2 cm^2

Figure 2.- Drawing of model used in investigation. All limear dimensions in centimeters.

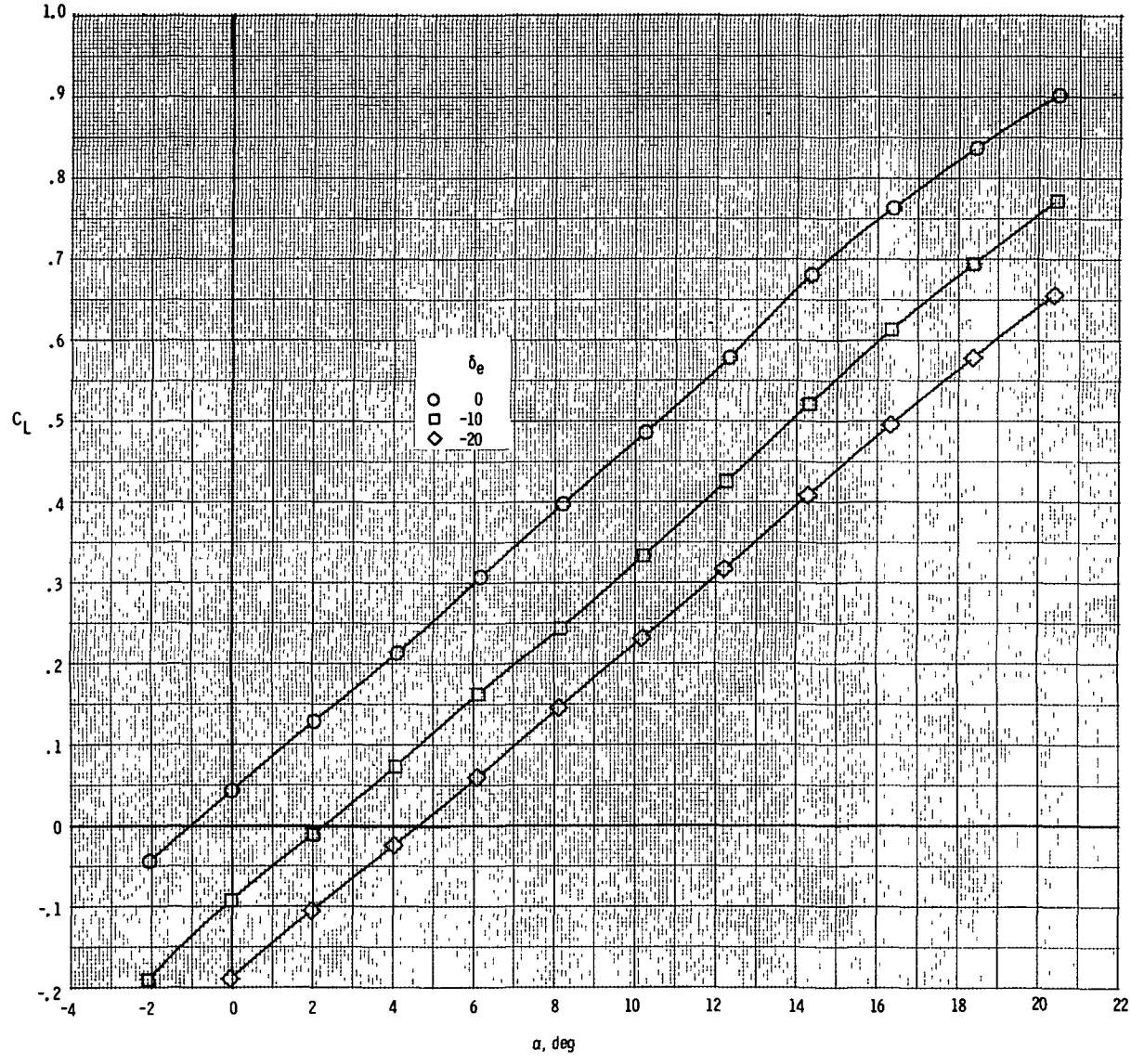

(a) C_L as a function of α. M = 0.3.

Figure 3.- Static longitudinal characteristics of model at M = 0.3.

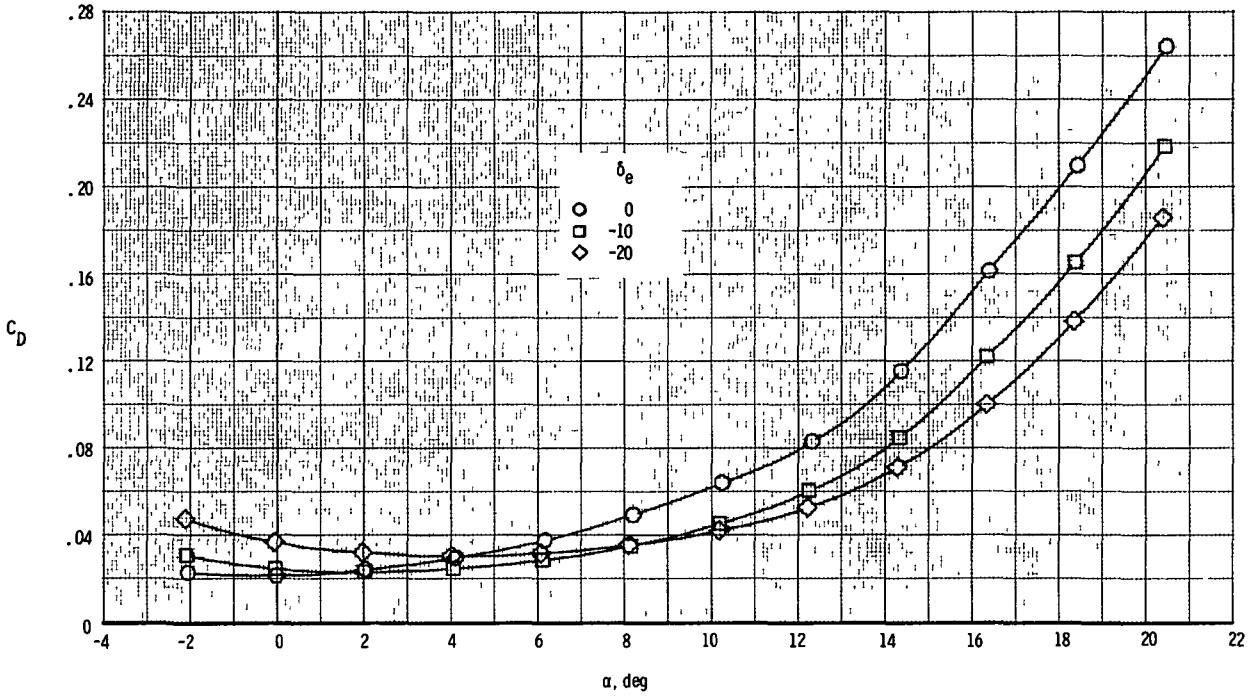

(b) C_D as a function of α. M = 0.3.

Figure 3.- Continued.

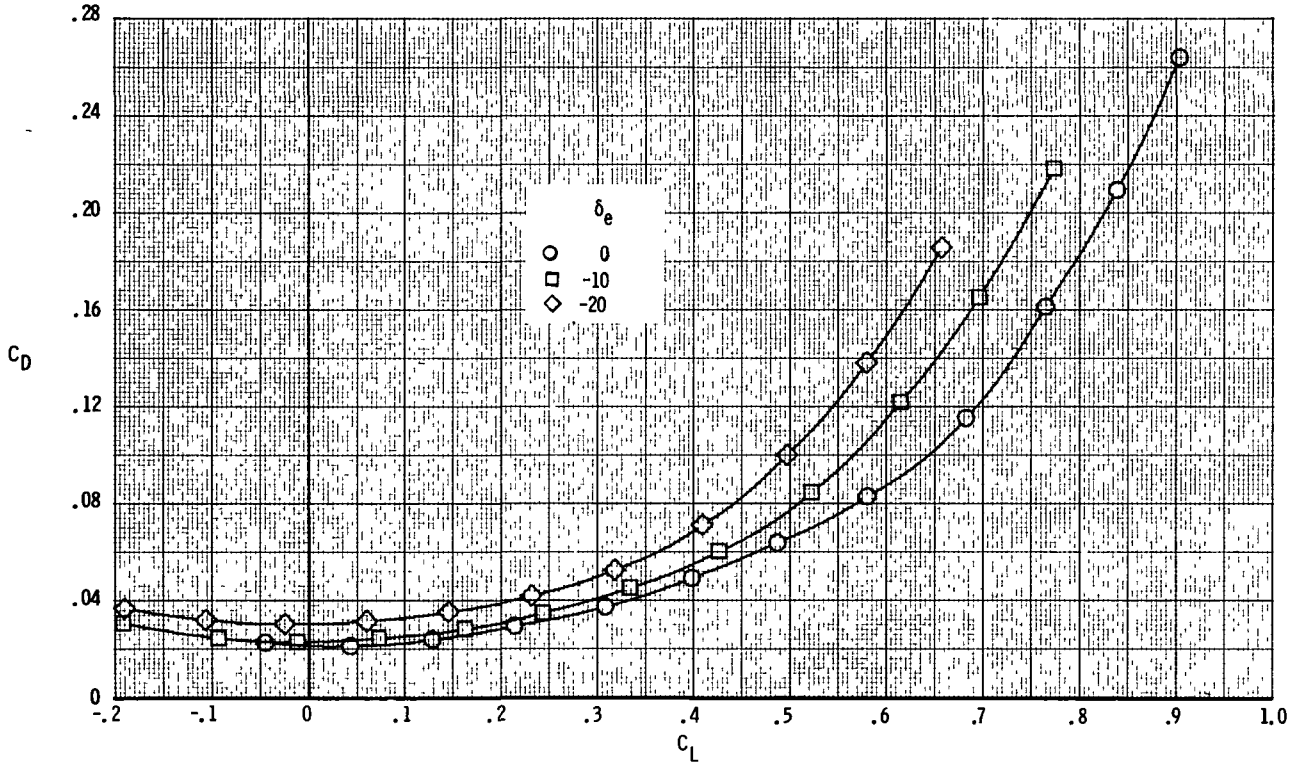

(c) C_D as a function of C_L. M = 0.3.

Figure 3.- Continued.

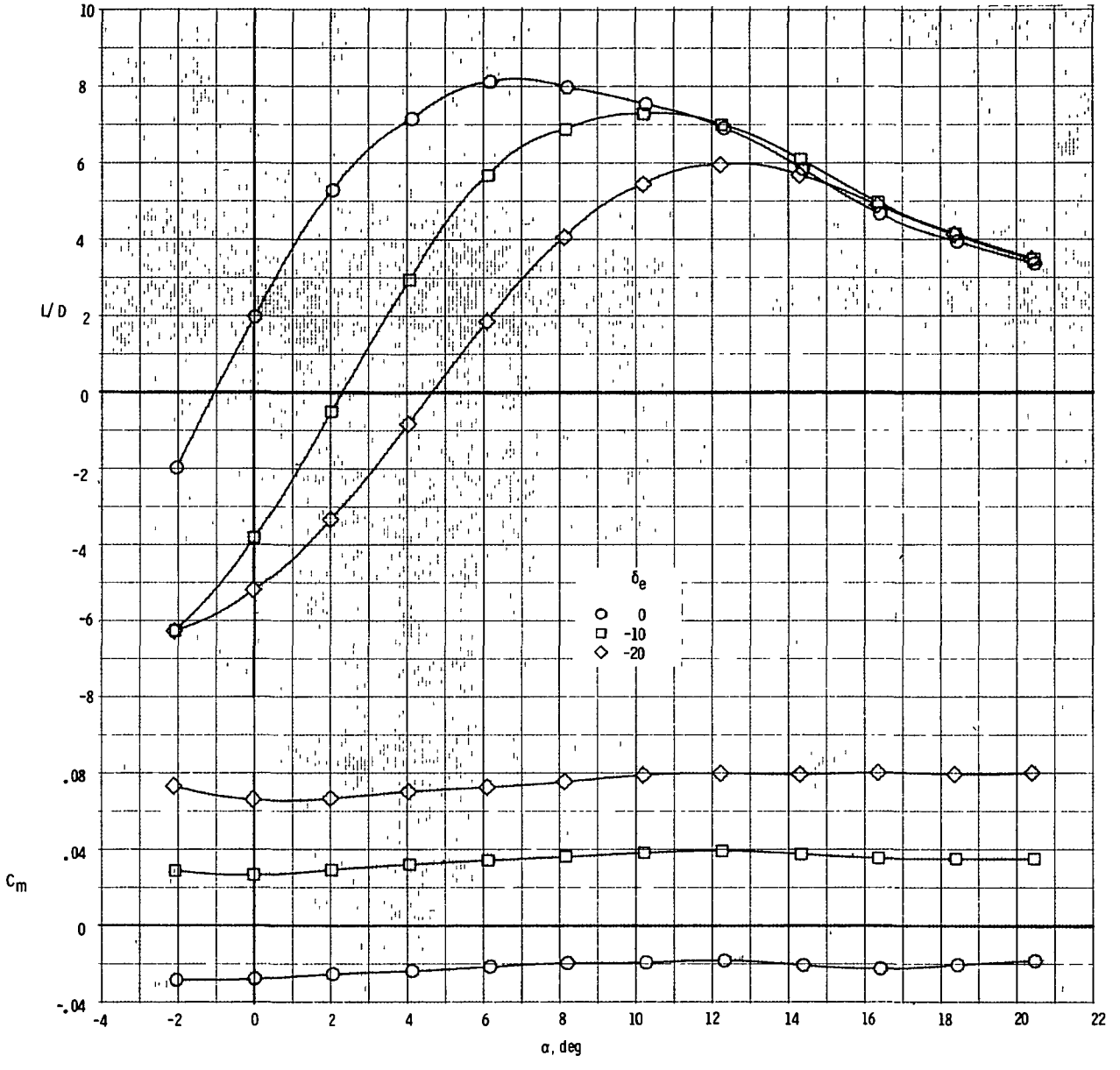

(d) C_m and L/D as functions of α. M = 0.3.

Figure 3.- Continued.

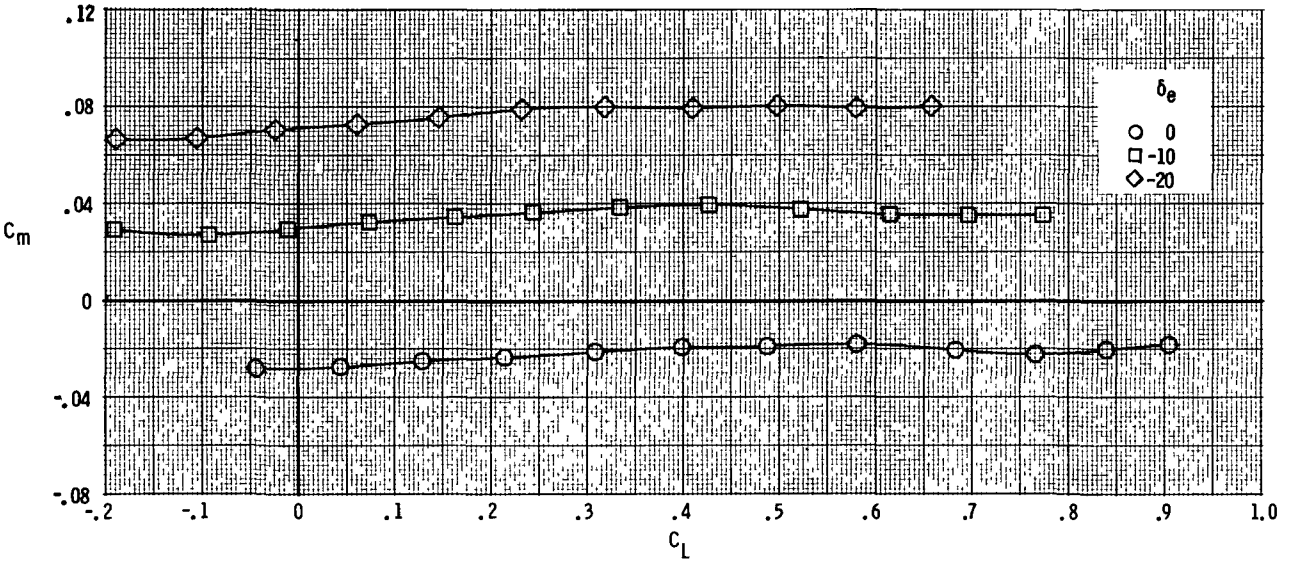

(e) C_m as a function of C_L. M = 0.3.

Figure 3.- Concluded.

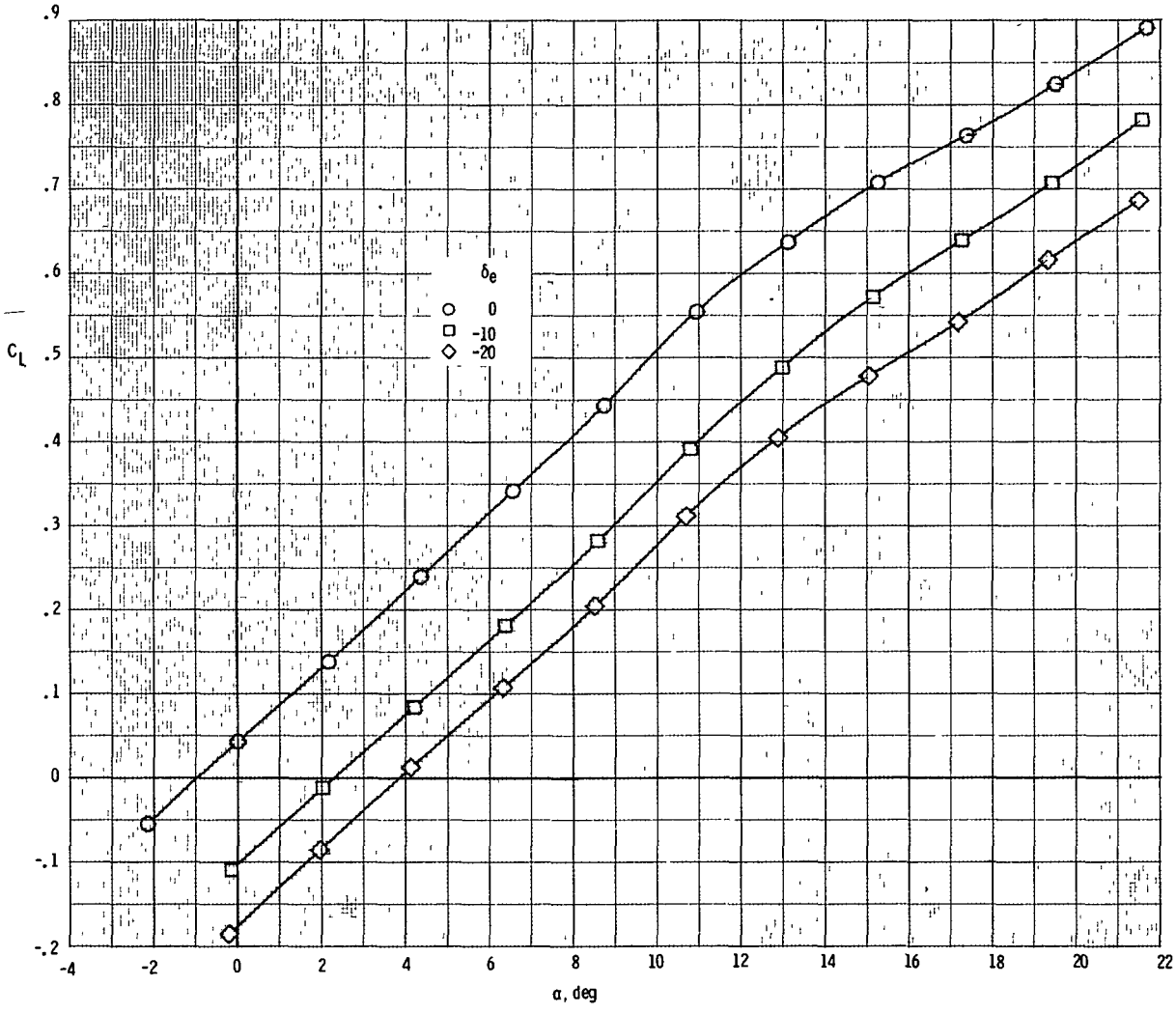

(a) C_L as a function of α. M = 0.6.

Figure 4.- Static longitudinal characteristics of model at M = 0.6.

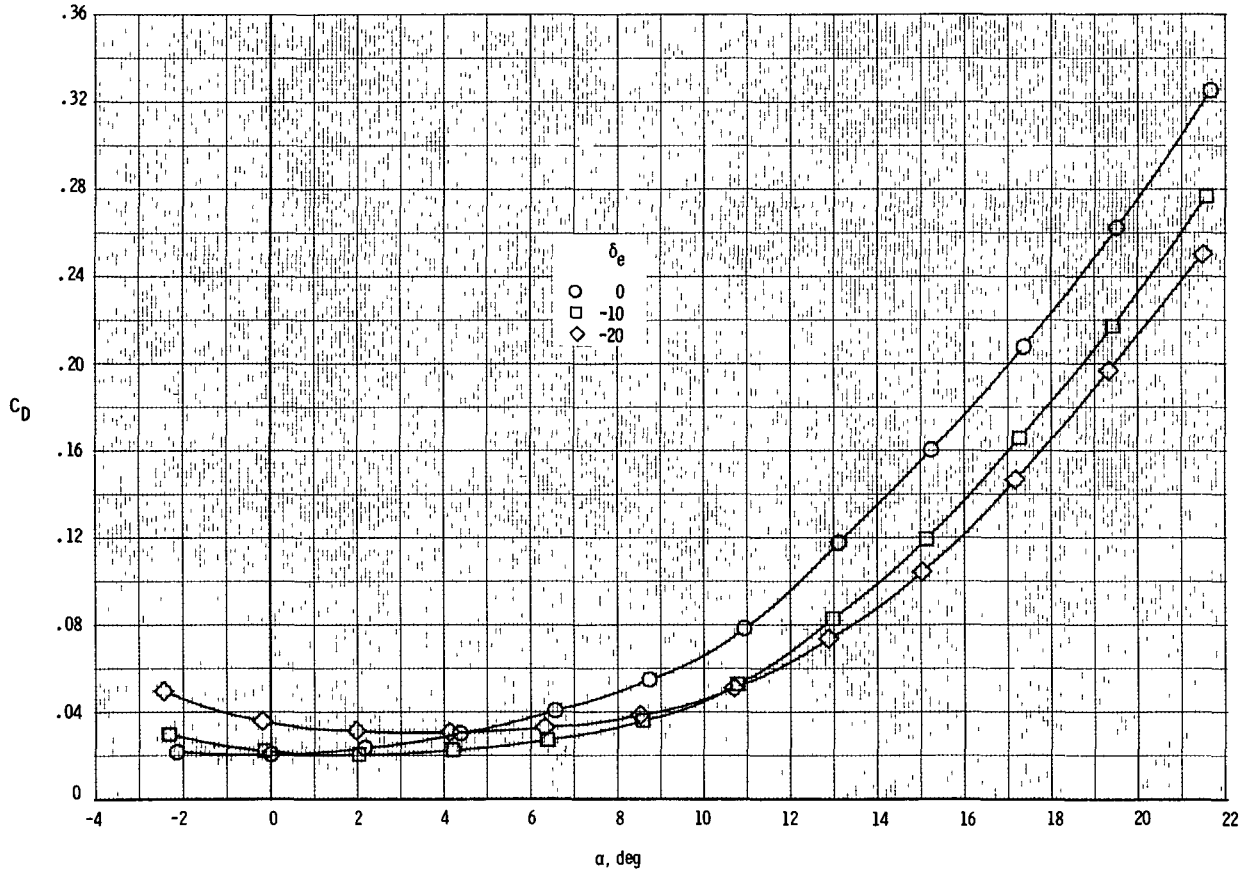

(b) C_D as a function of α. M = 0.6.

Figure 4.- Continued.

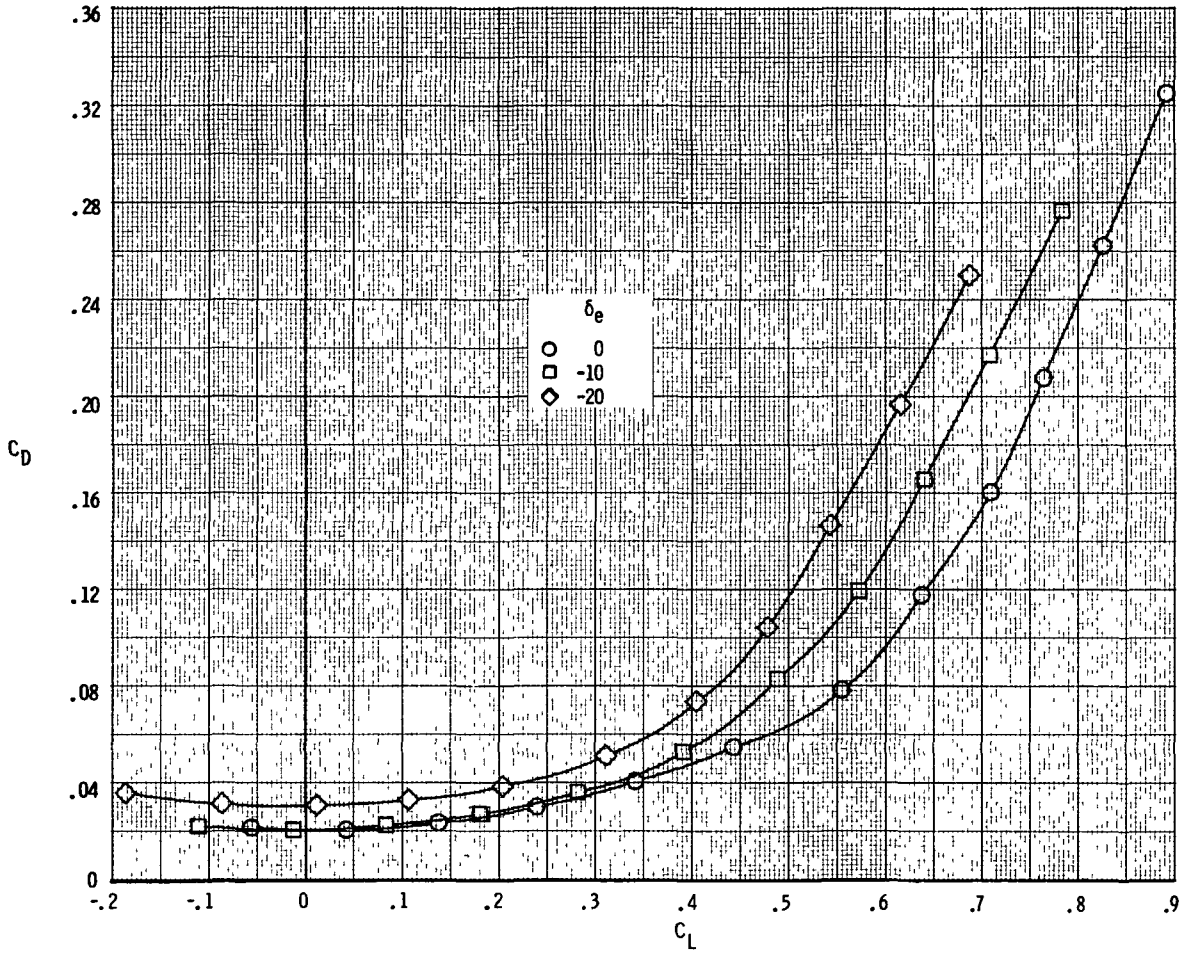

(c) C_D as a function of C_L. M = 0.6.

Figure 4.- Continued.

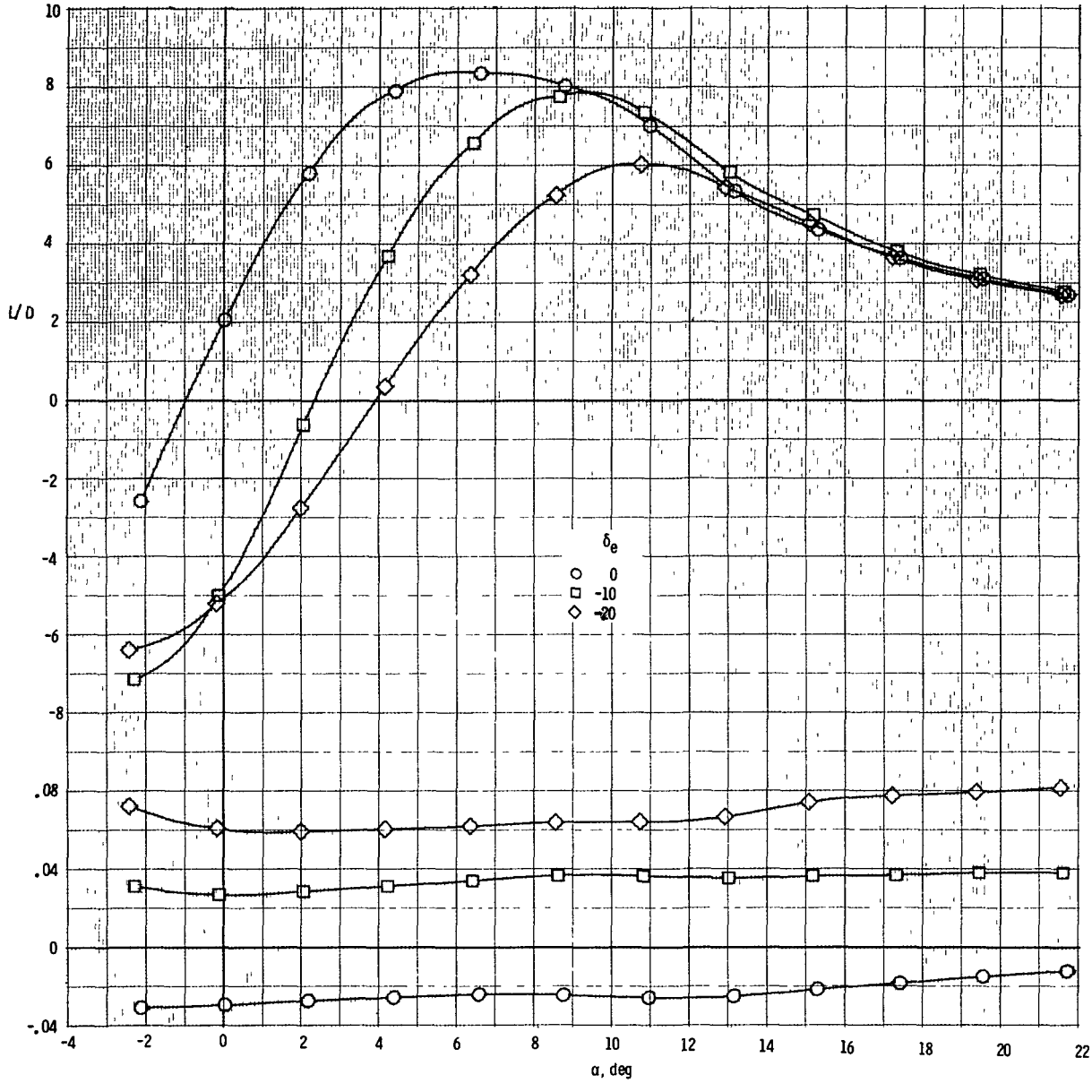

(d) C_m and L/D as functions of α. M = 0.6.

Figure 4.- Continued.

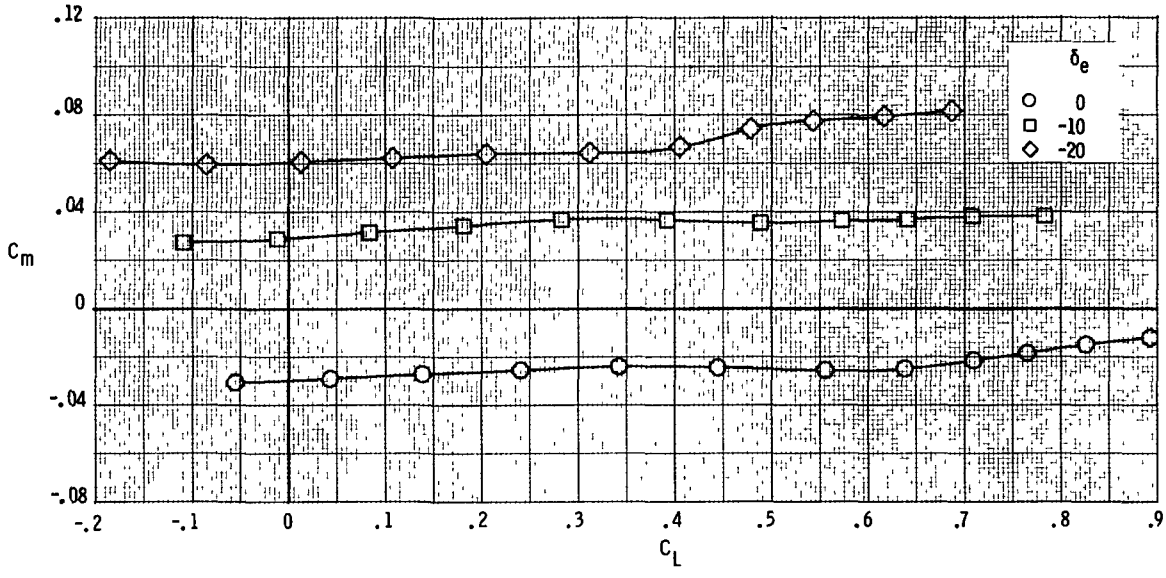

(e) C_m as a function of C_L. M = 0.6.

Figure 4.- Concluded.

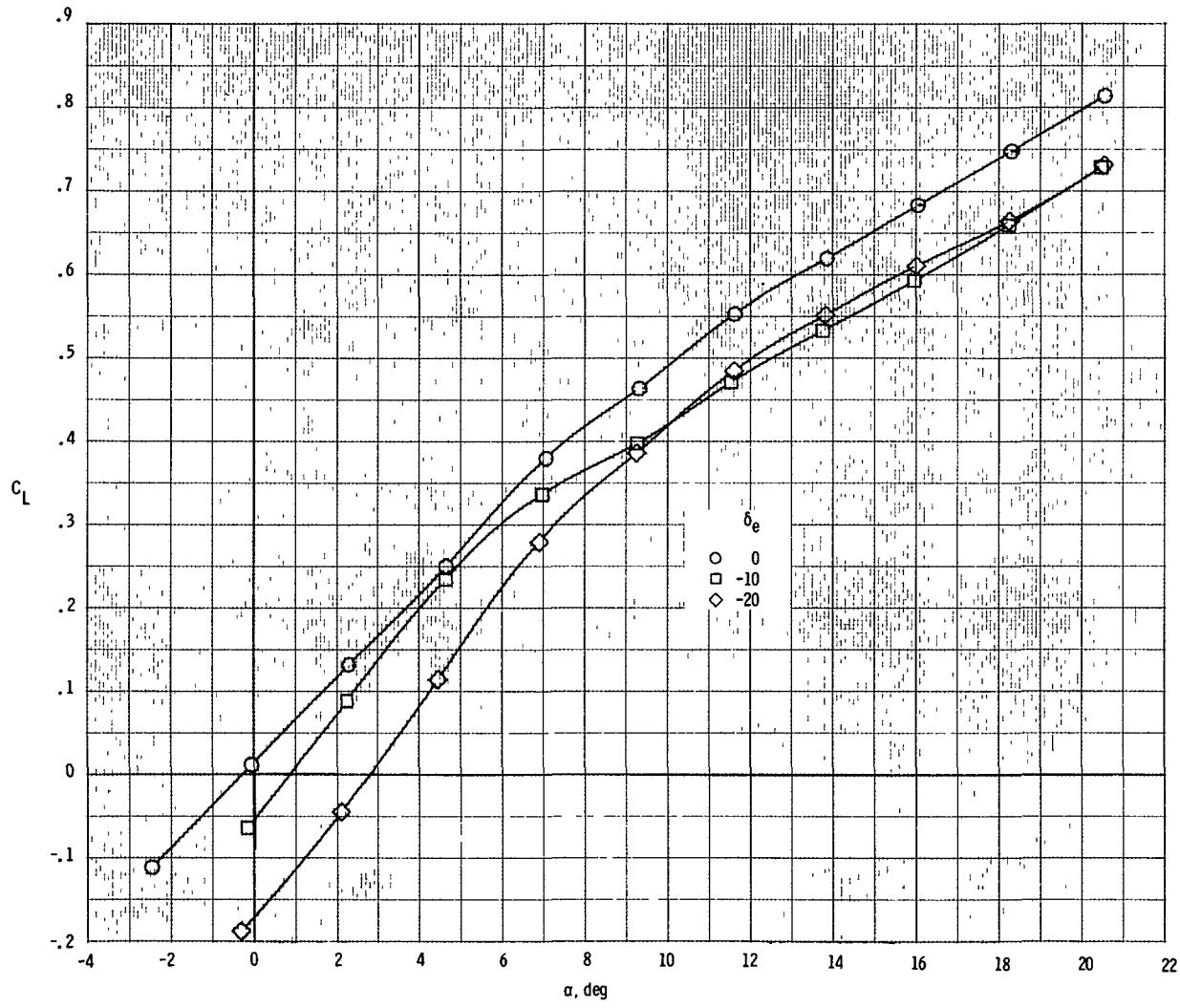

(a) C_L as a function of α. M = 0.9.

Figure 5.- Static longitudinal characteristics of model at M = 0.9.

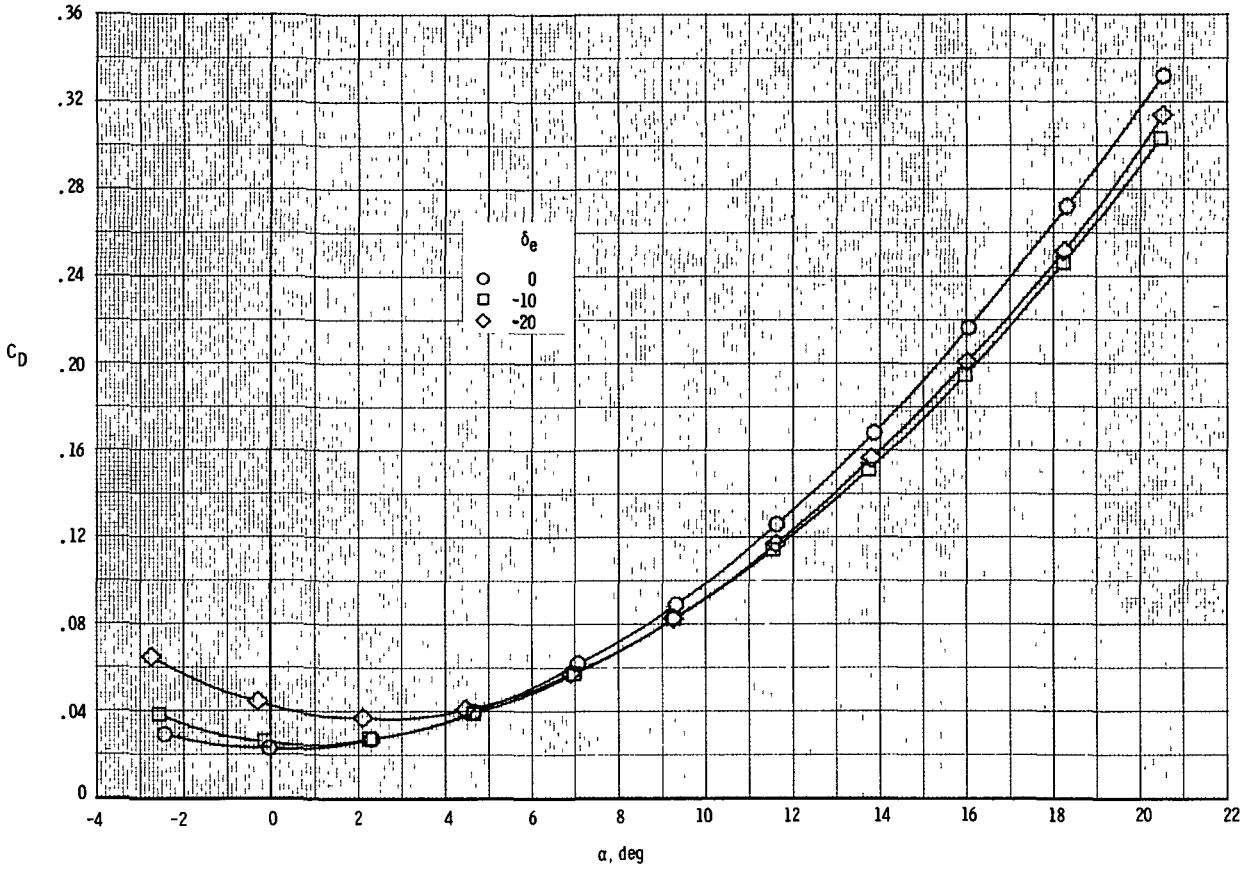

(b) C_D as a function of α. M = 0.9.

Figure 5.- Continued.

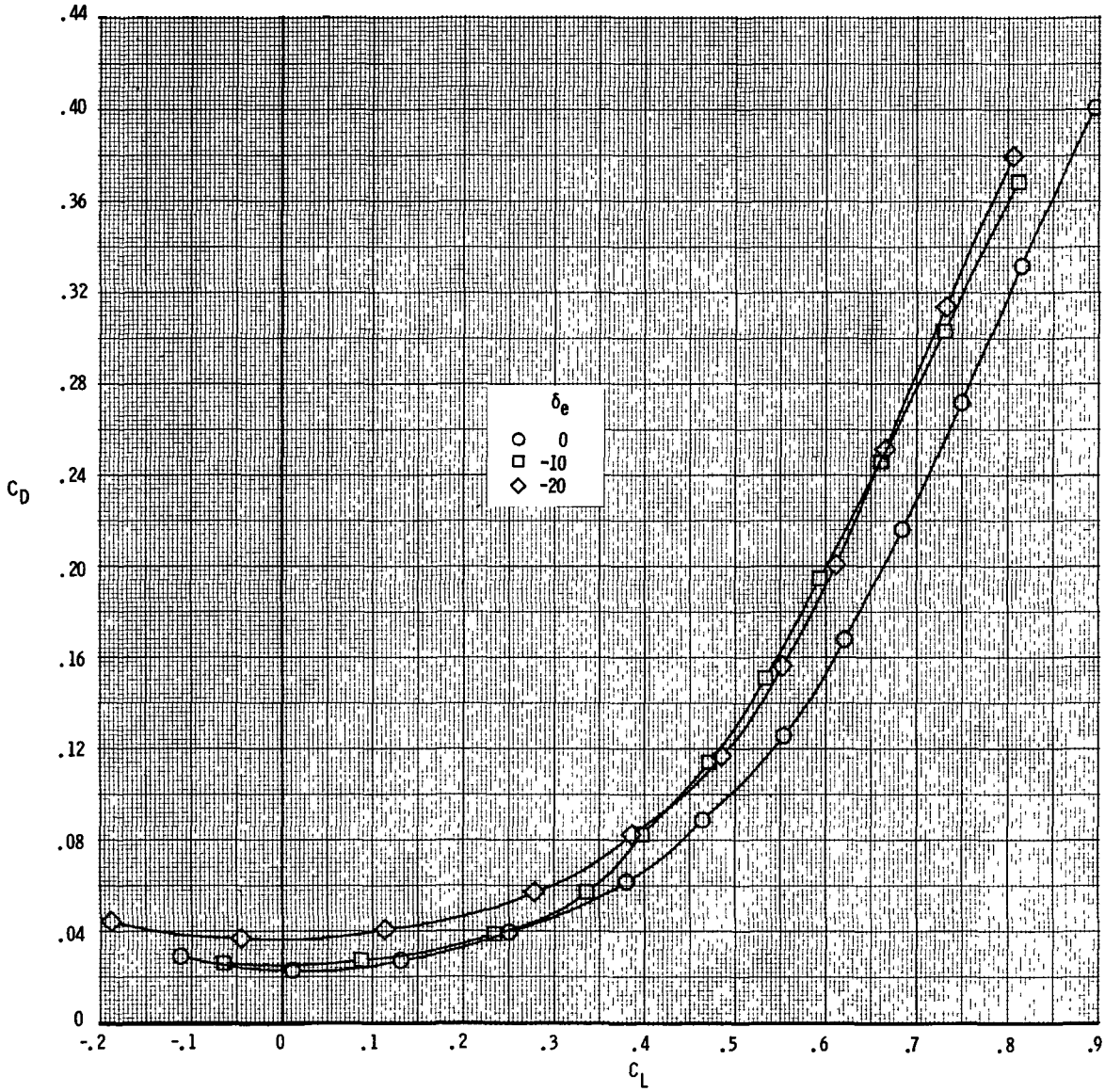

(c) C_D as a function of C_L. M = 0.9.

Figure 5.- Continued.

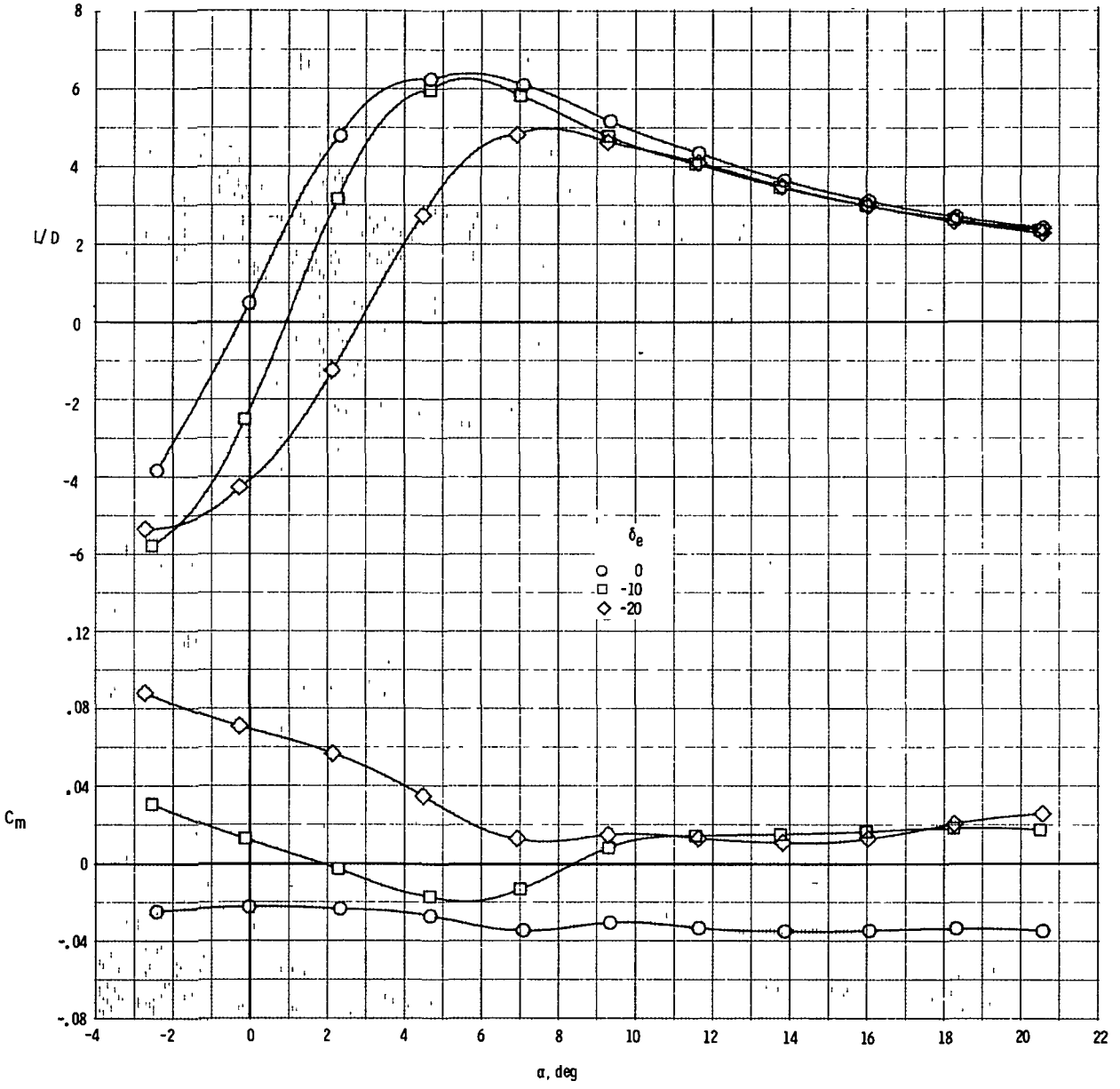

(d) C_m and L/D as functions of α. M = 0.9.

Figure 5.- Continued.

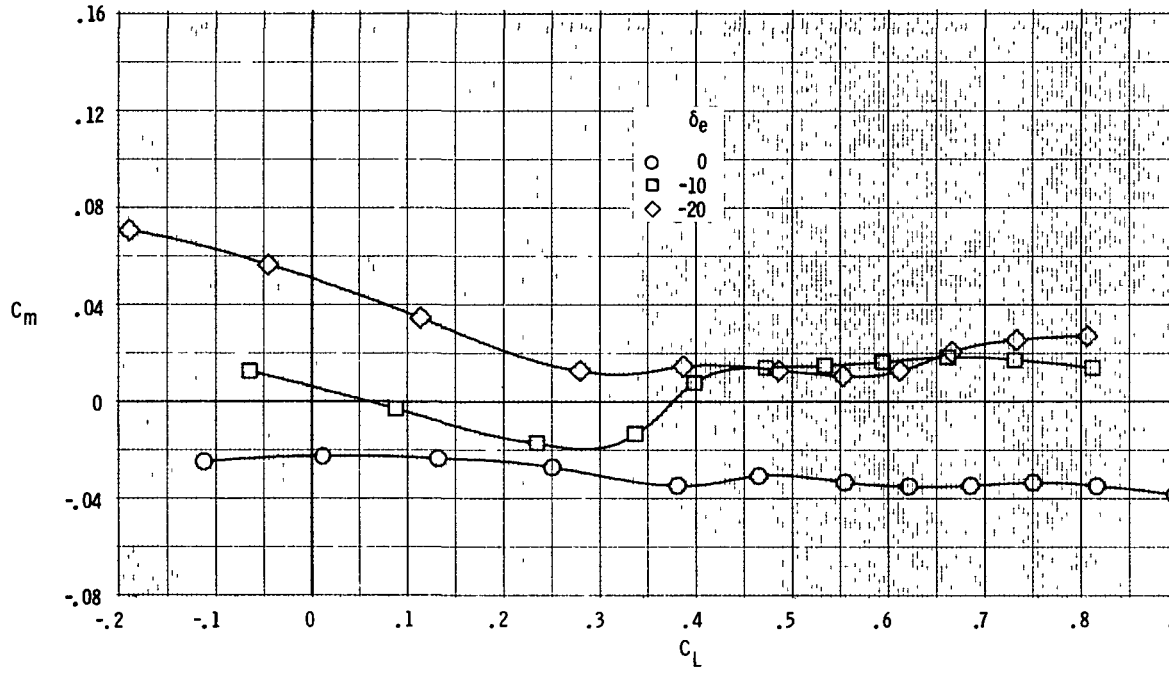

(e) C_m as a function of C_L. M = 0.9.

Figure 5.- Concluded.

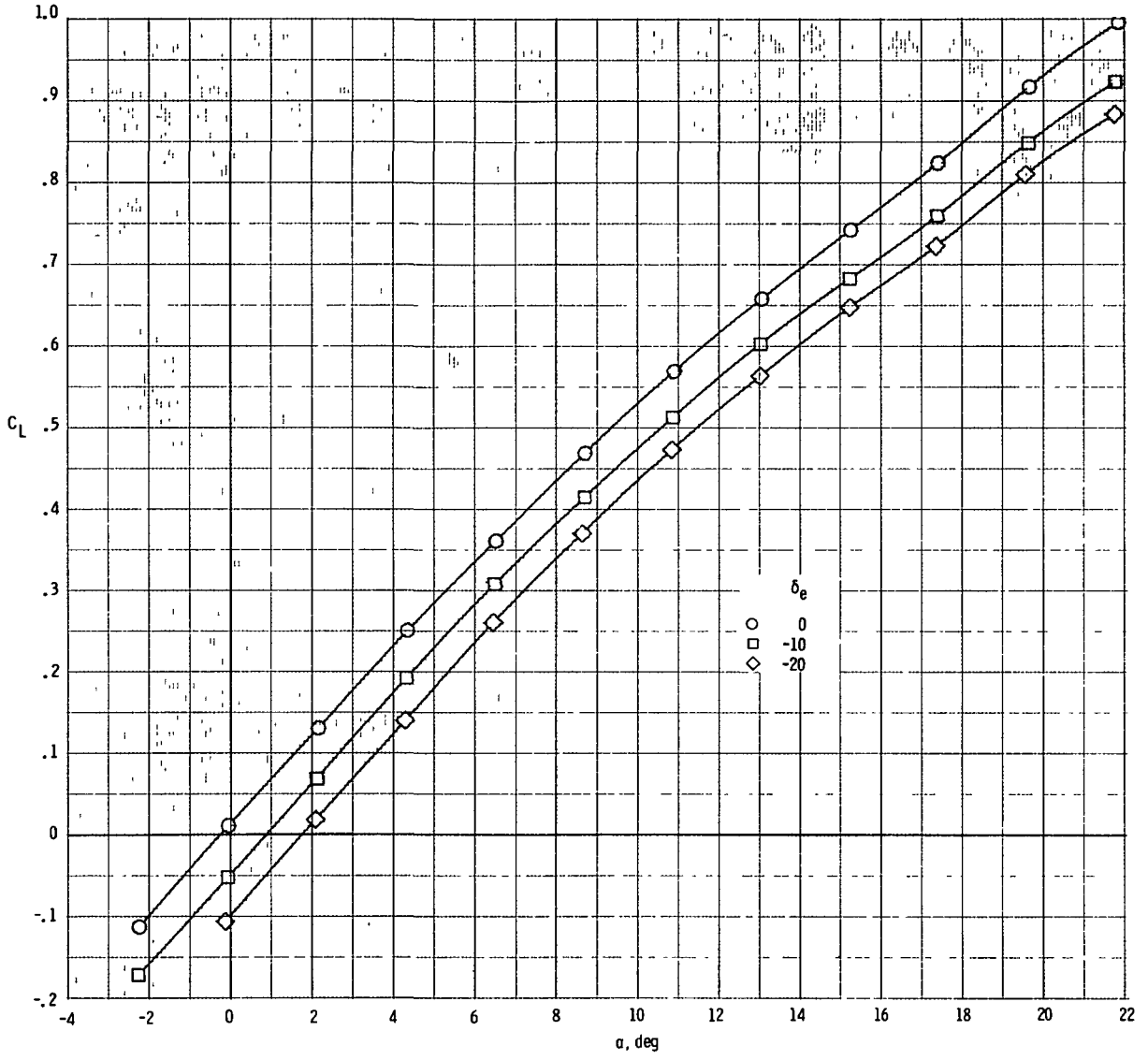

(a) C_L as a function of α. M = 1.2.

Figure 6.- Static longitudinal characteristics of model at M = 1.2.

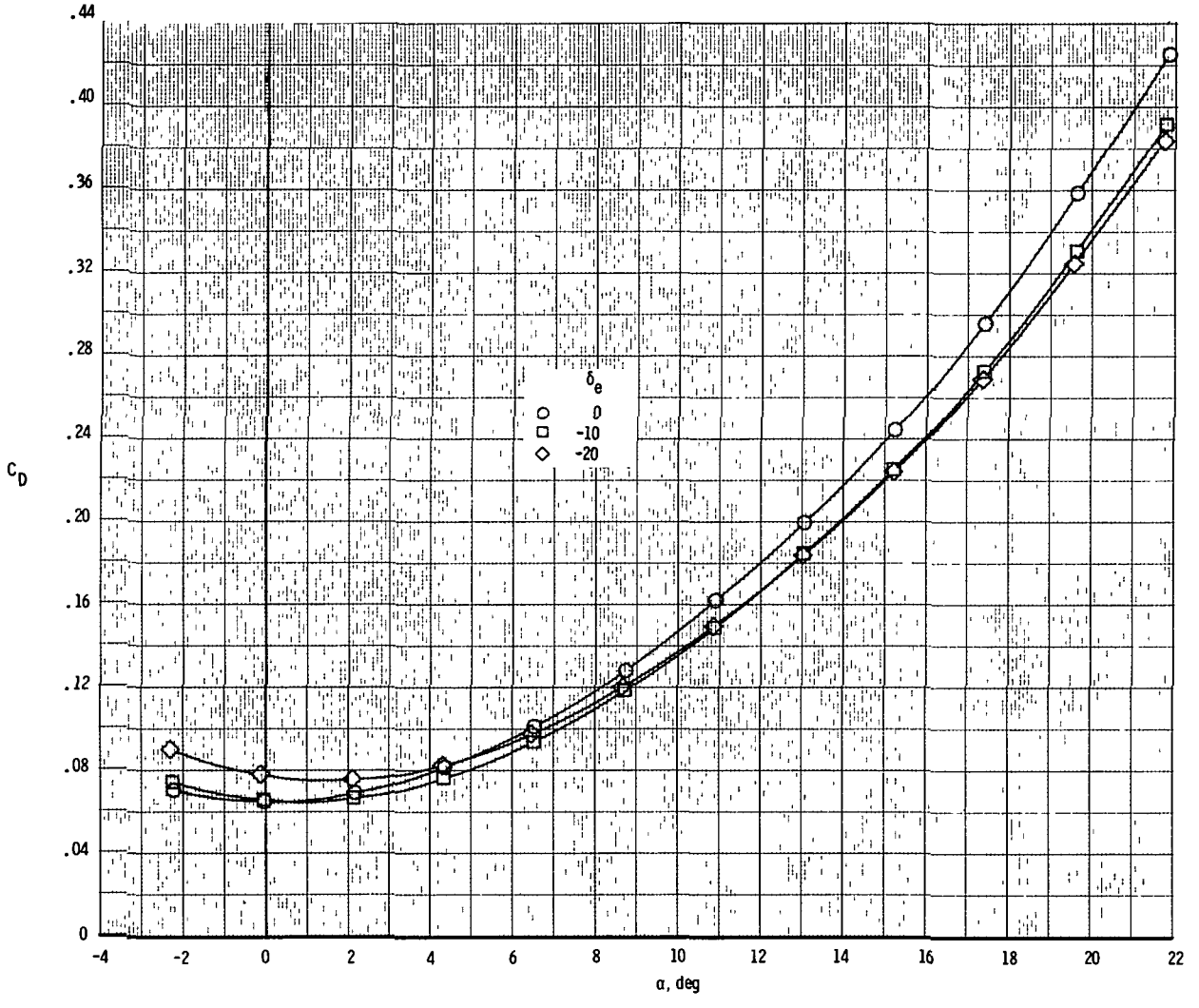

(b) C_D as a function of α. M = 1.2.

Figure 6.- Continued.

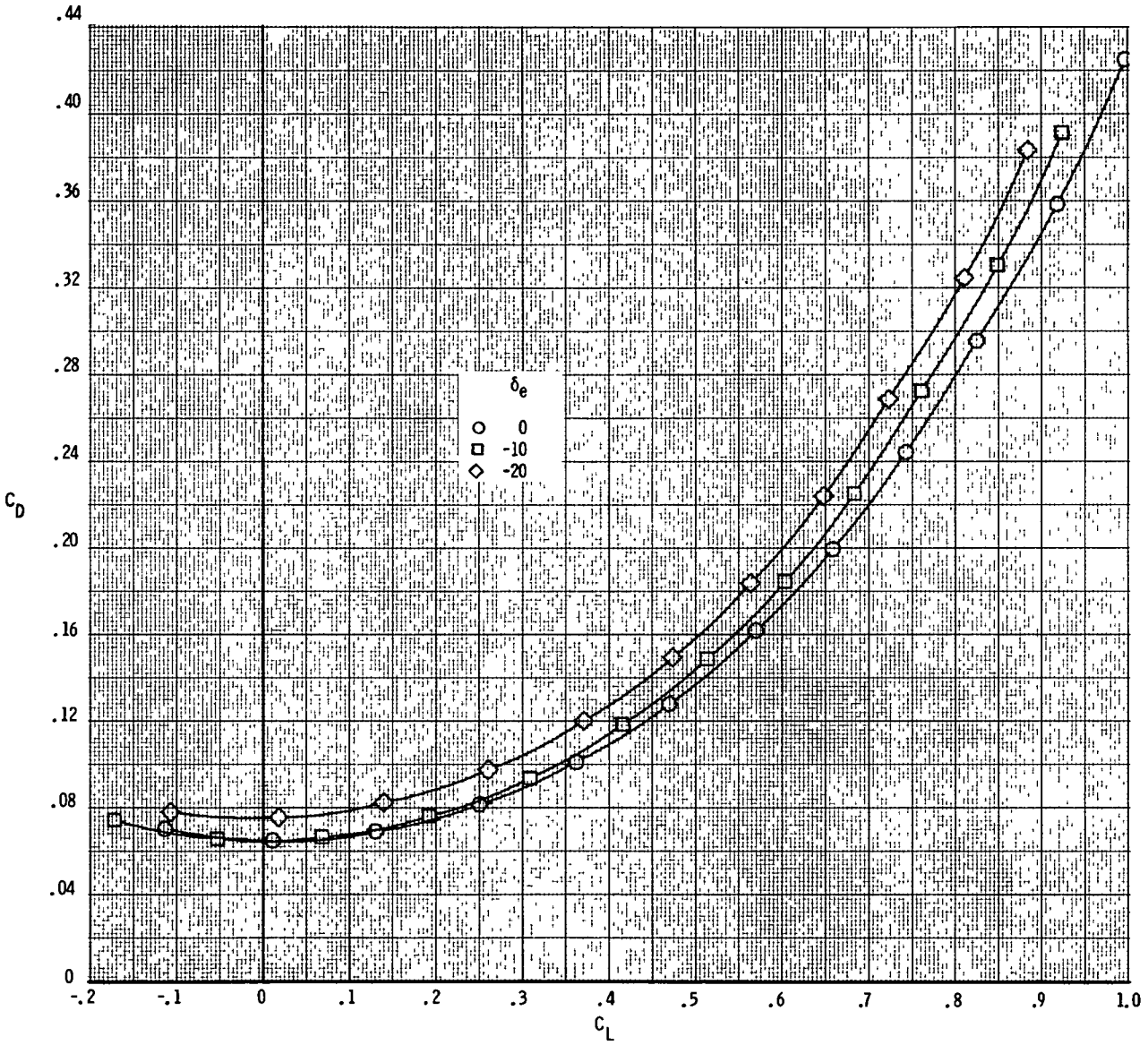

(c) C_D as a function of C_L. M = 1.2.

Figure 6.- Continued.

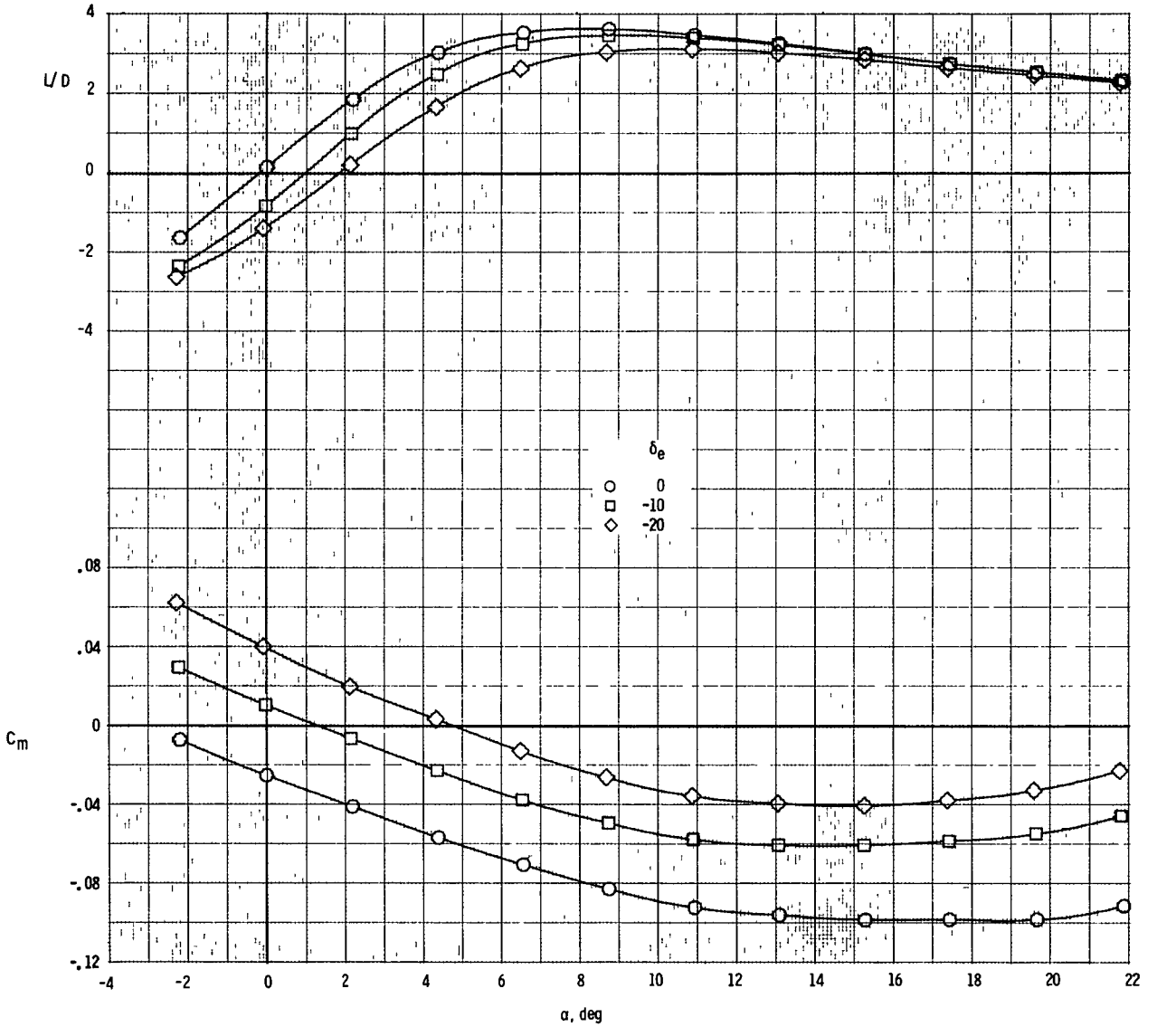

(d) C_m and L/D as functions of α. M = 1.2.

Figure 6.- Continued.

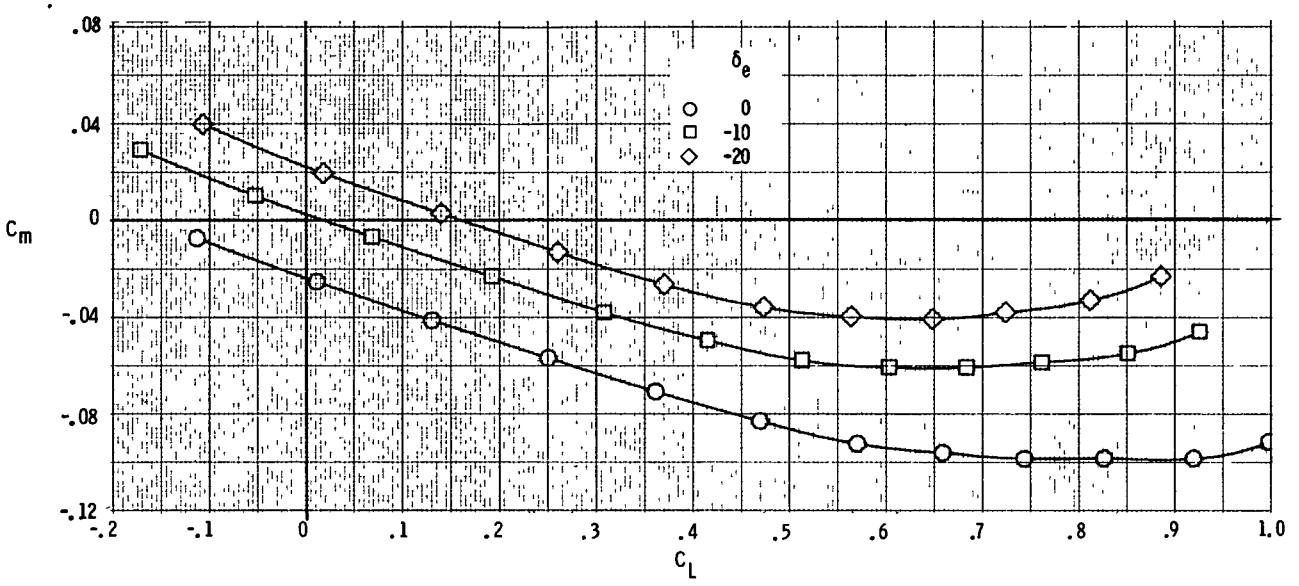

(e) C_m as a function of C_L. M = 1.2.

Figure 6.- Concluded.

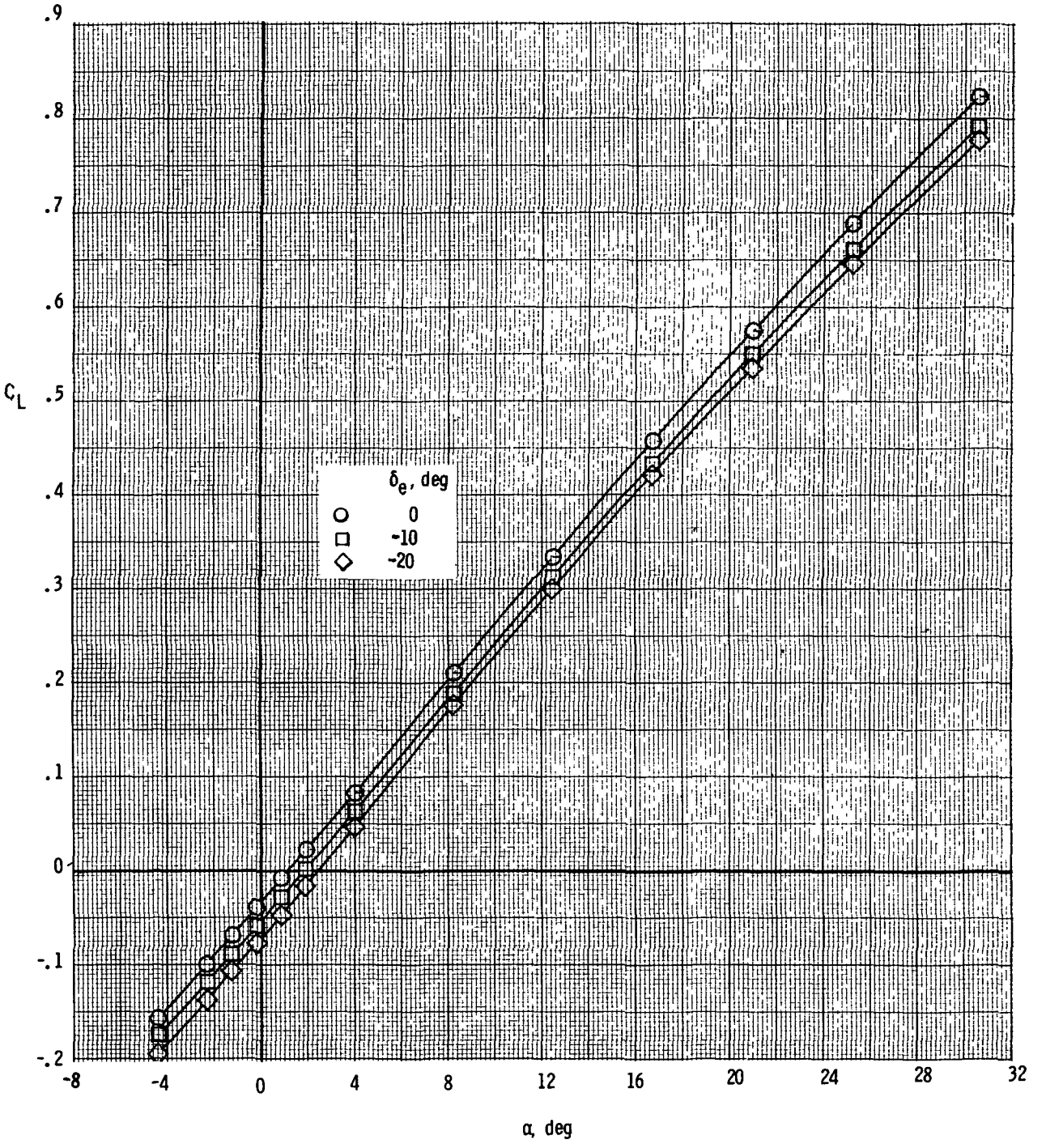

(a) C_L as a function of α. M = 2.36.

Figure 7.- Static longitudinal stability and trim characteristics at M = 2.36.

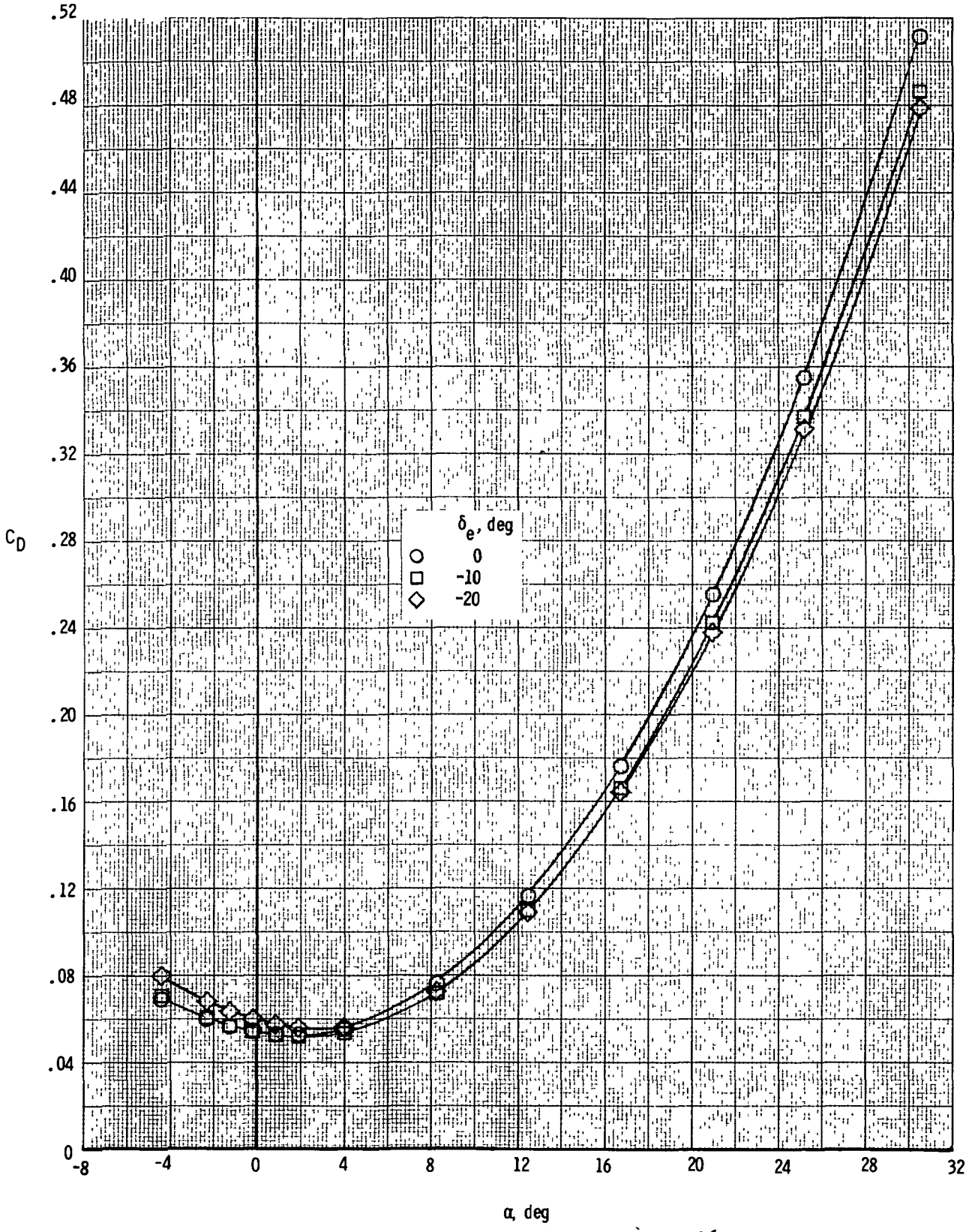

(b) C_D as a function of α. $M = 2.36$.

Figure 7.- Continued.

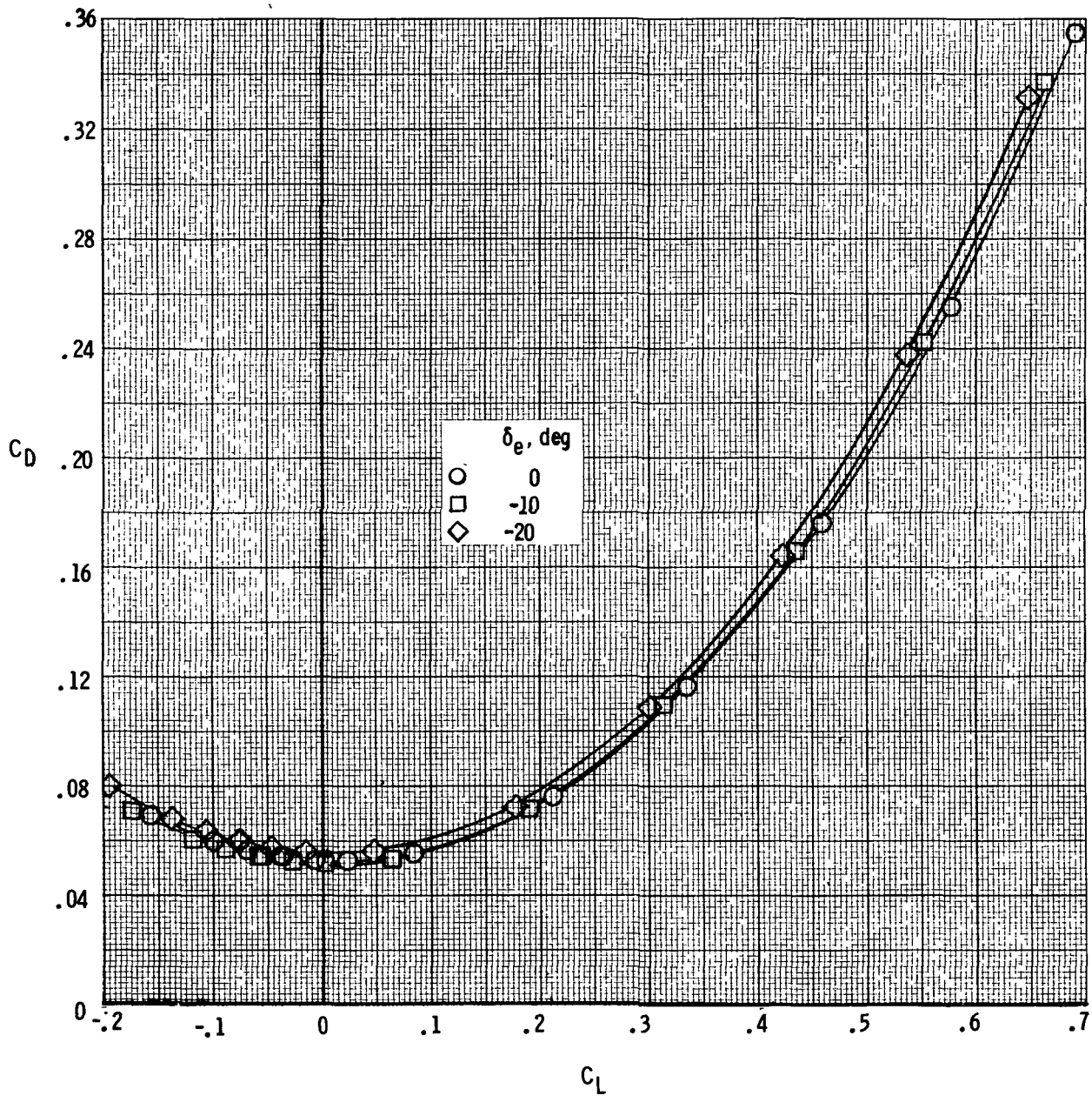

(c) C_D as a function of C_L. M = 2.36.

Figure 7.- Continued.

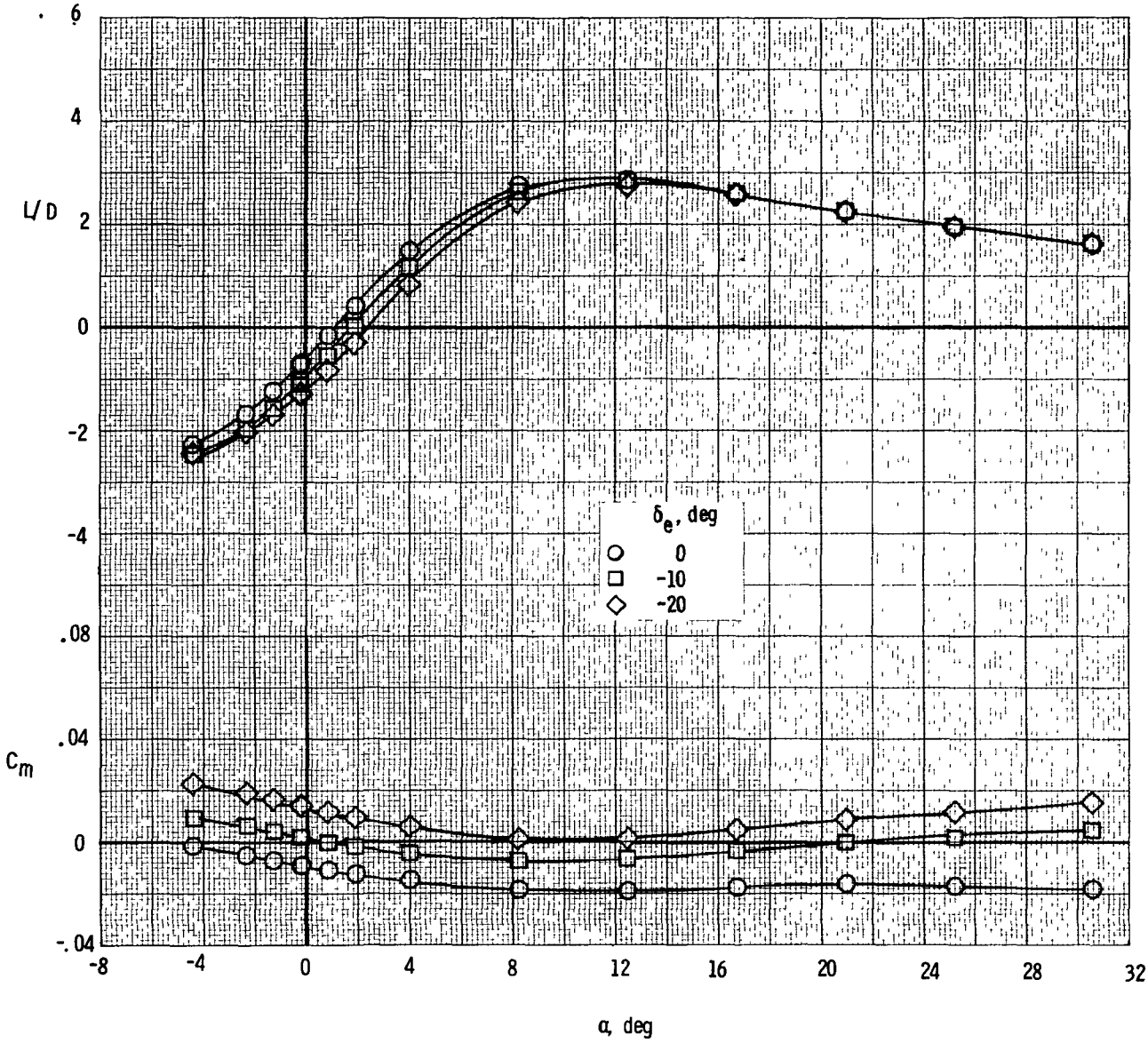

(d) C_m and L/D as functions of α. M = 2.36.

Figure 7.- Continued.

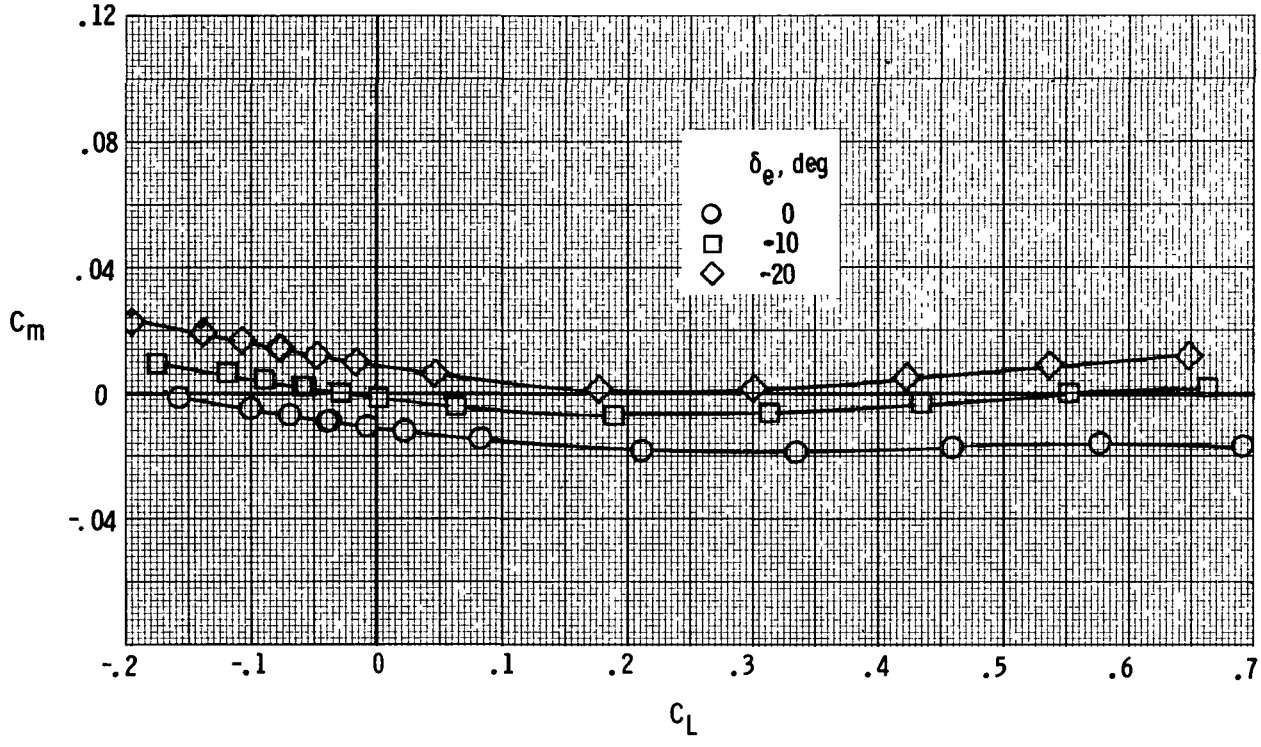

(e) C_m as a function of C_L. M = 2.36.

Figure 7.- Concluded.

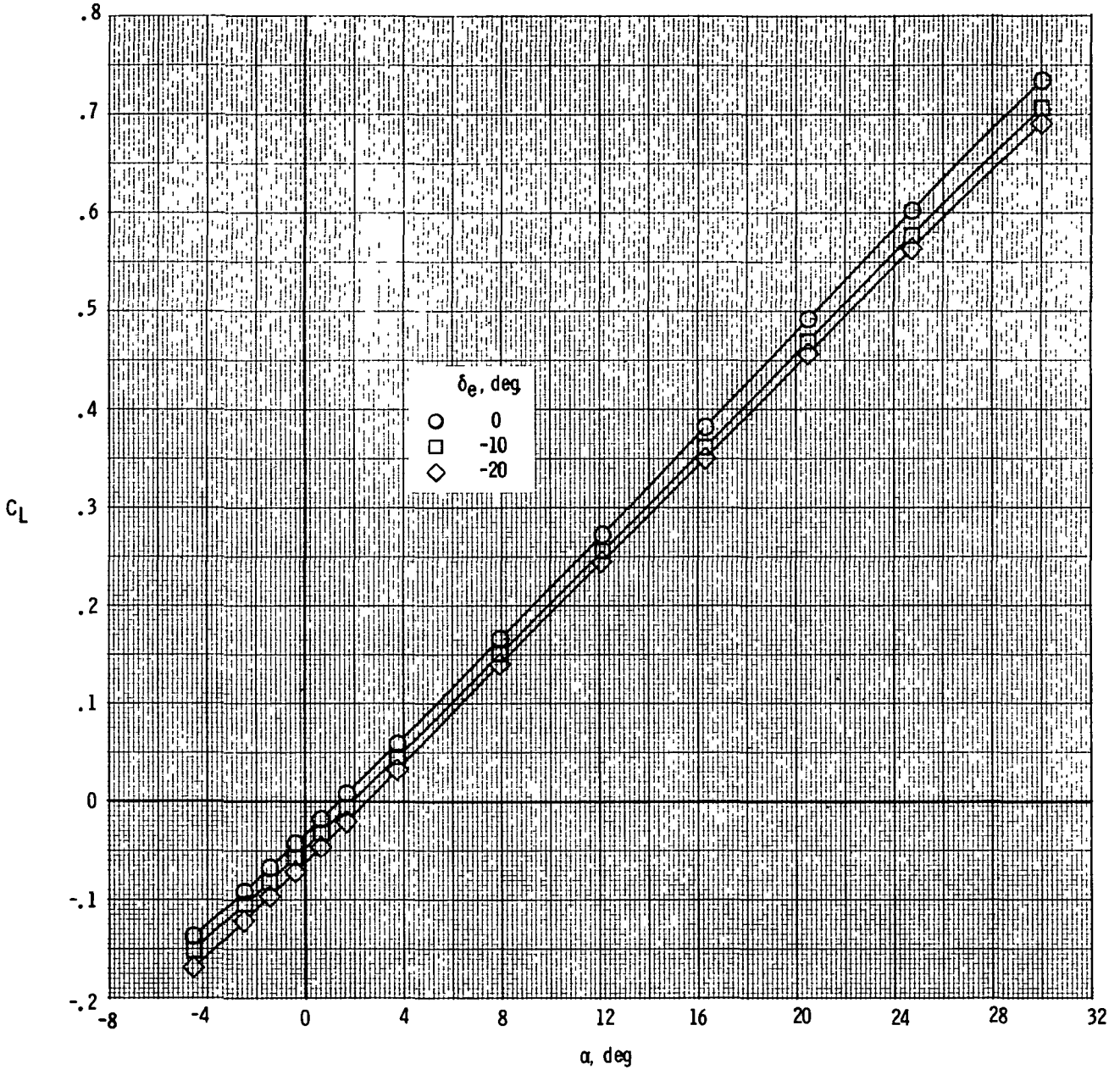

(a) C_L as a function of α. M = 2.86.

Figure 8.- Static longitudinal stability and trim characteristics at M = 2.86.

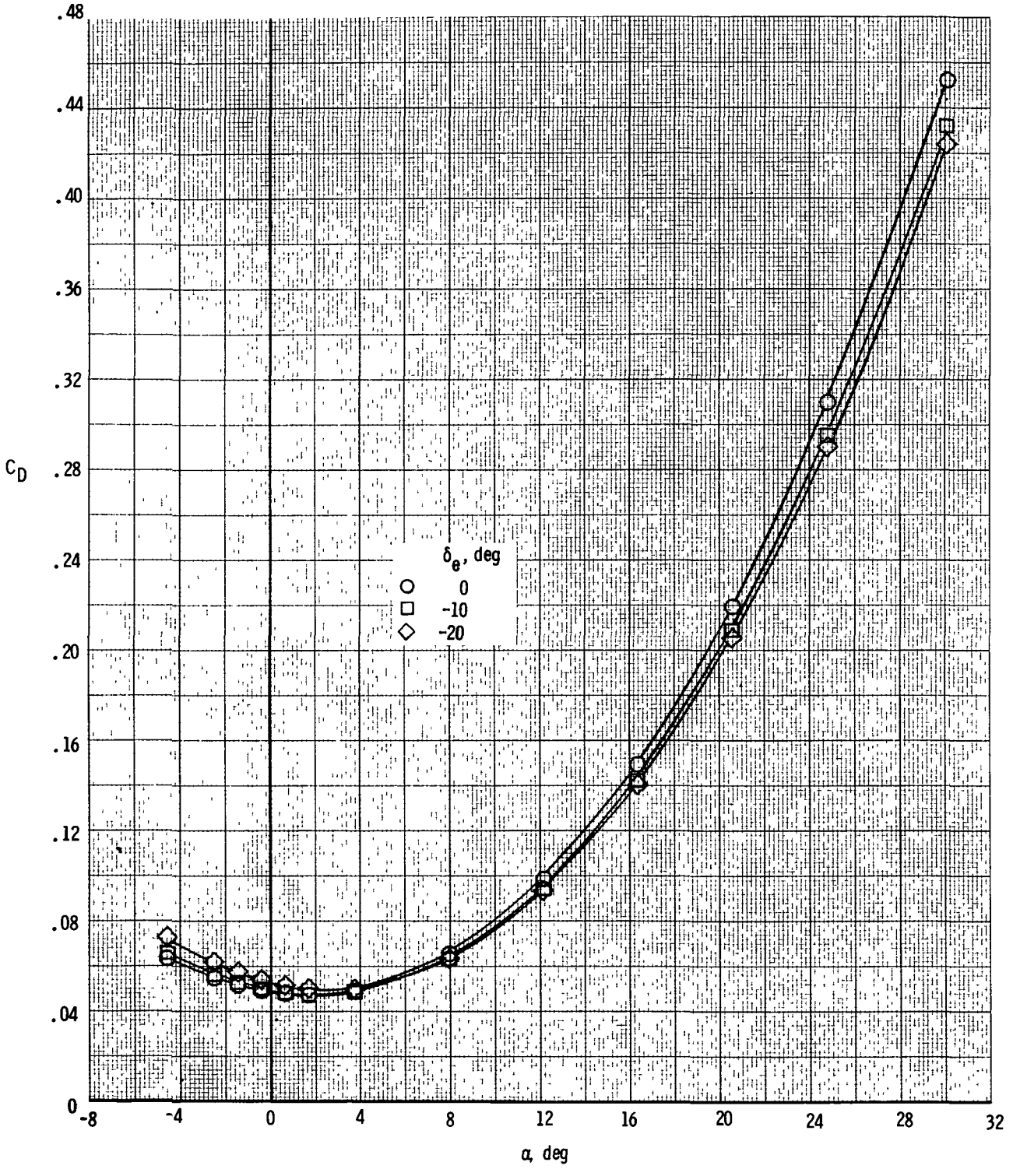

(b) C_D as a function of α. M = 2.86.

Figure 8.- Continued.

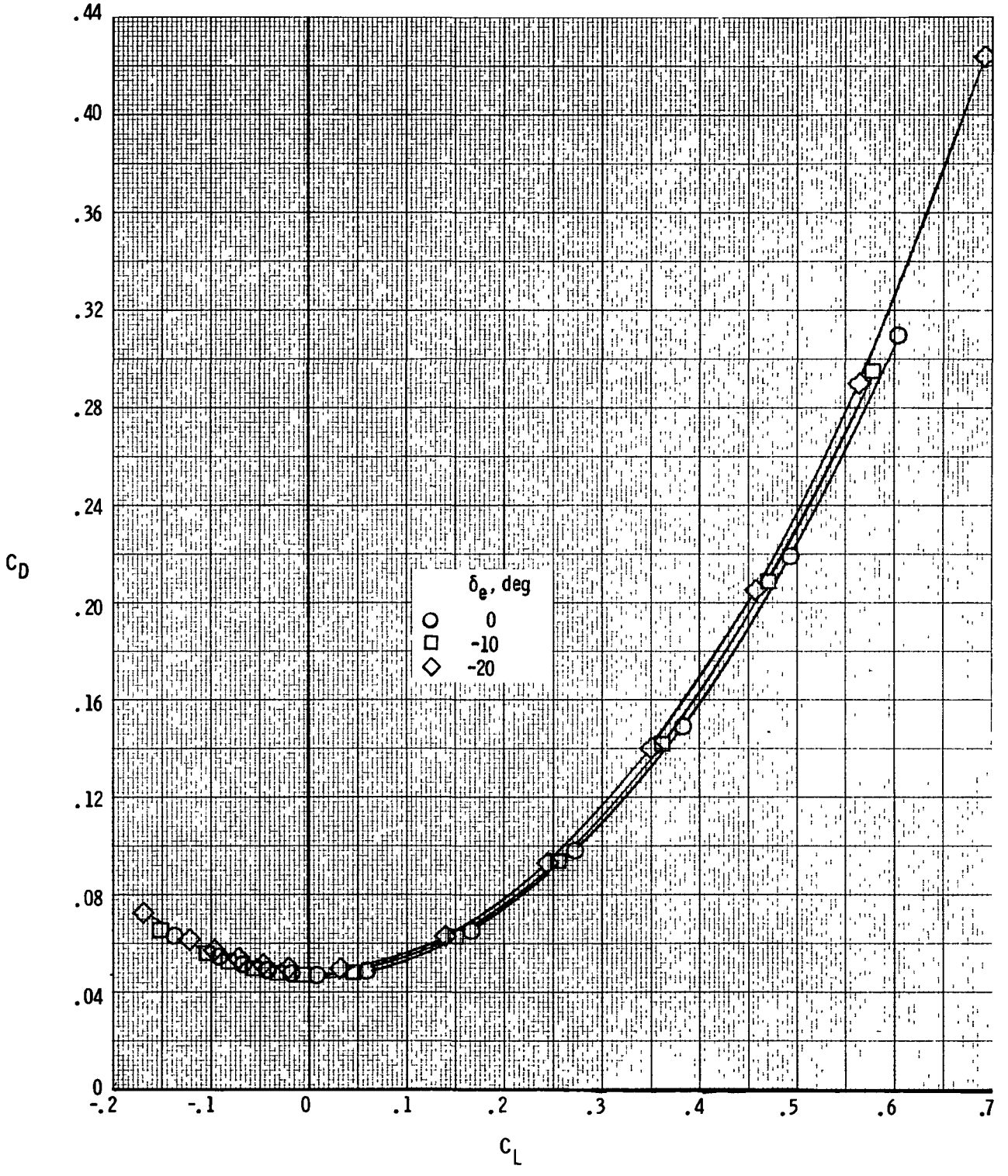

(c) C_D as a function of C_L. M = 2.86.

Figure 8.- Continued.

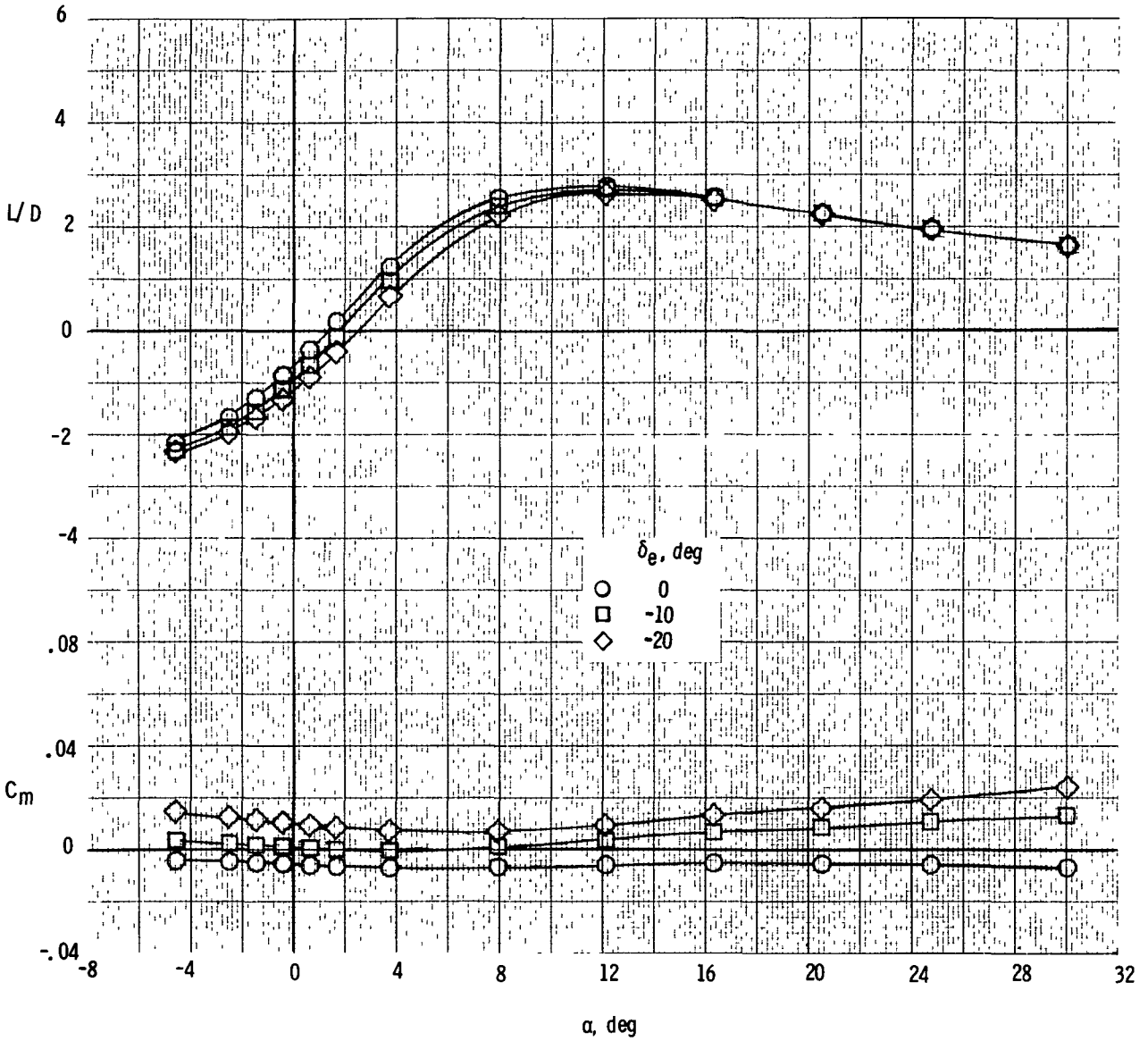

(d) C_m and L/D as functions of α. M = 2.86.

Figure 8.- Continued.

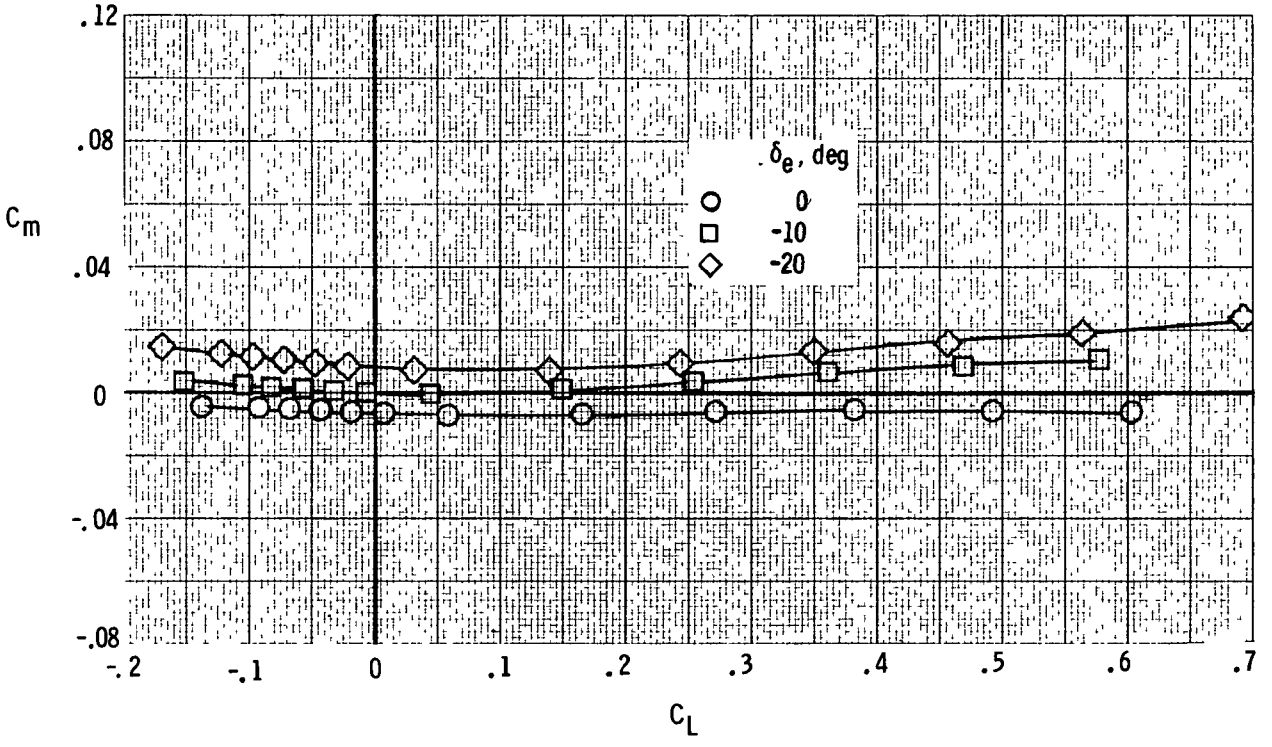

(e) C_m as a function of C_L. M = 2.86.

Figure 8.- Concluded.

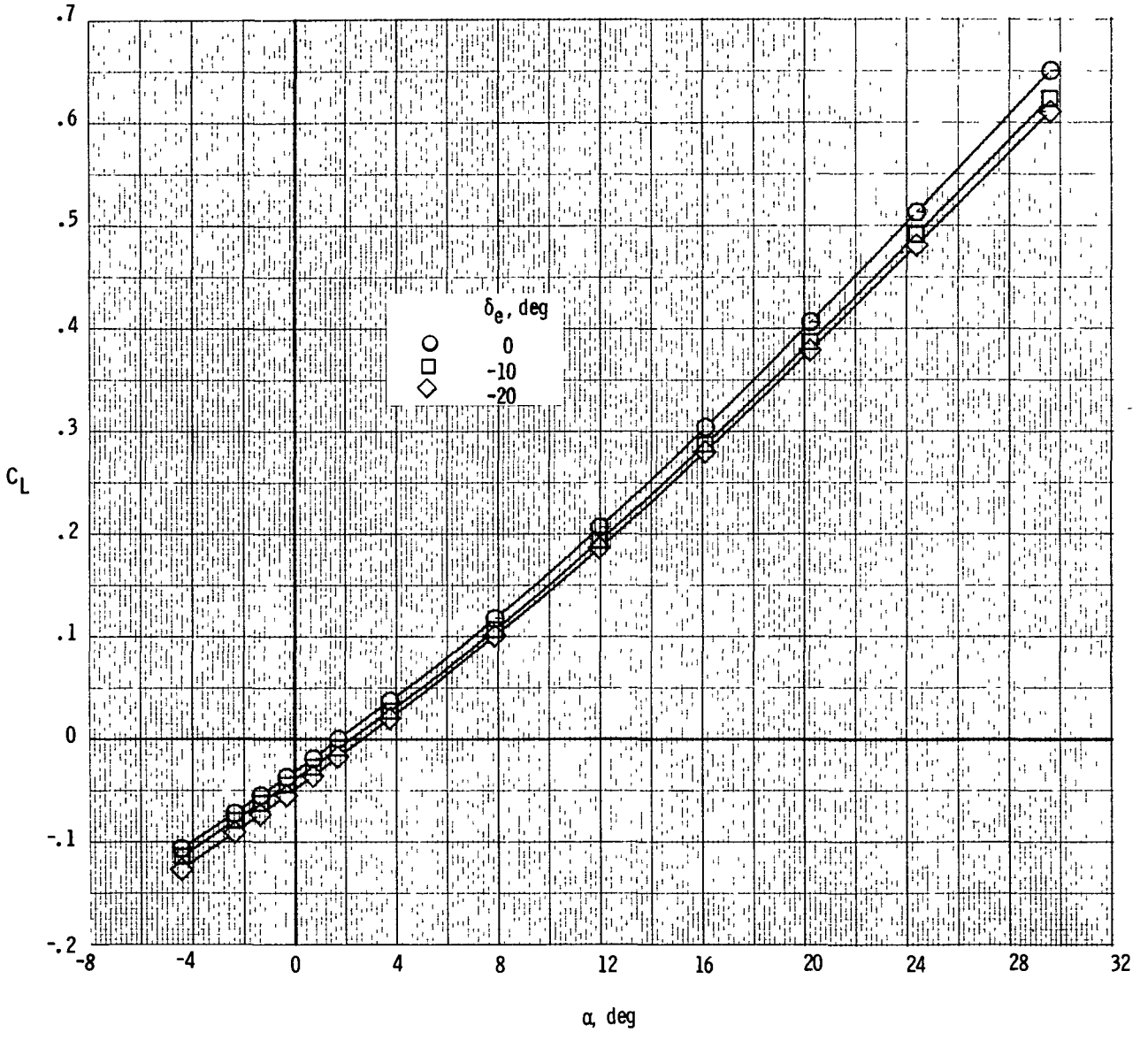

(a) C_L as a function of α. M = 3.95.

Figure 9.- Static longitudinal stability and trim characteristics at M = 3.95.

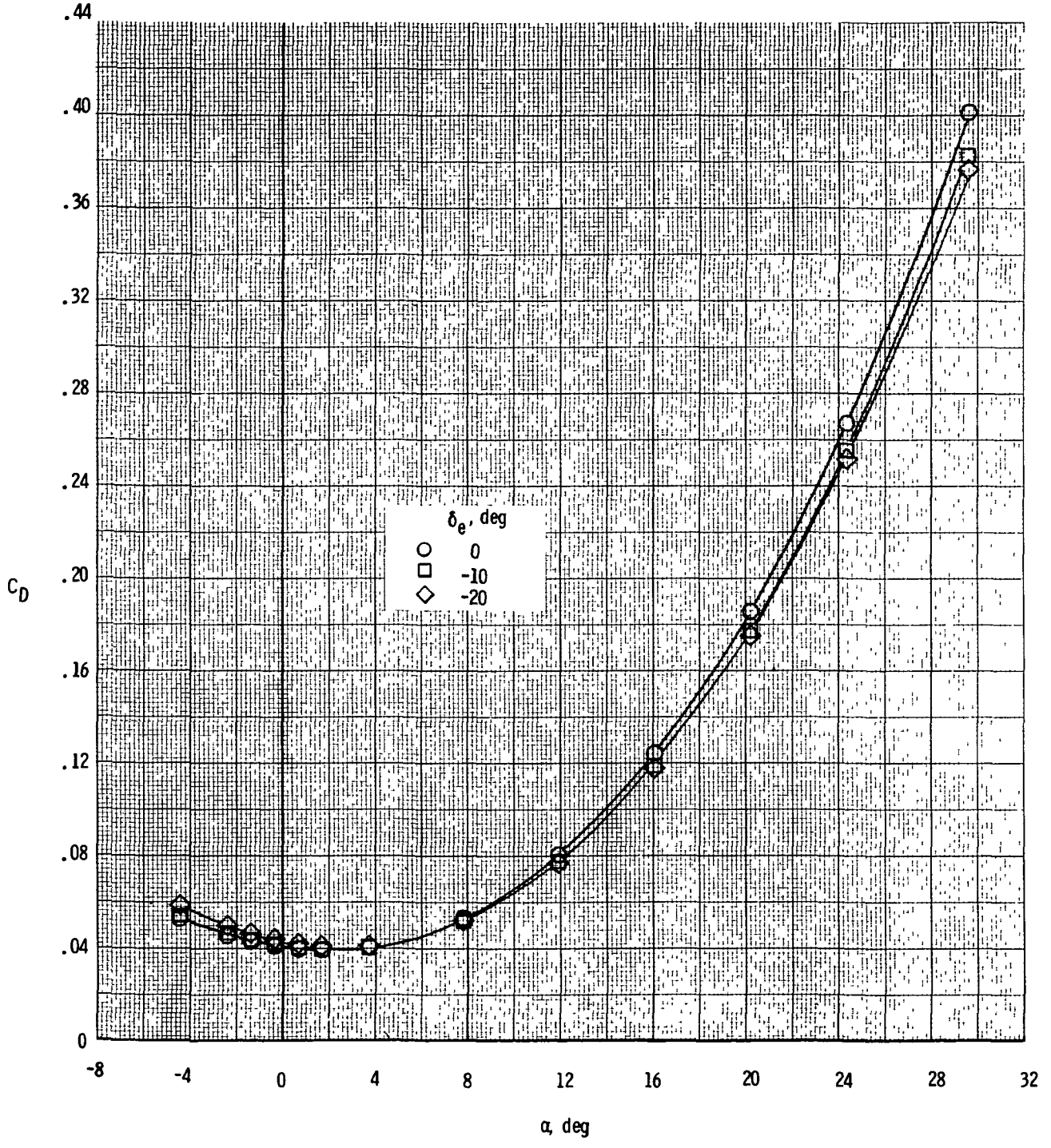

(b) C_D as a function of α. M = 3.95.

Figure 9.- Continued.

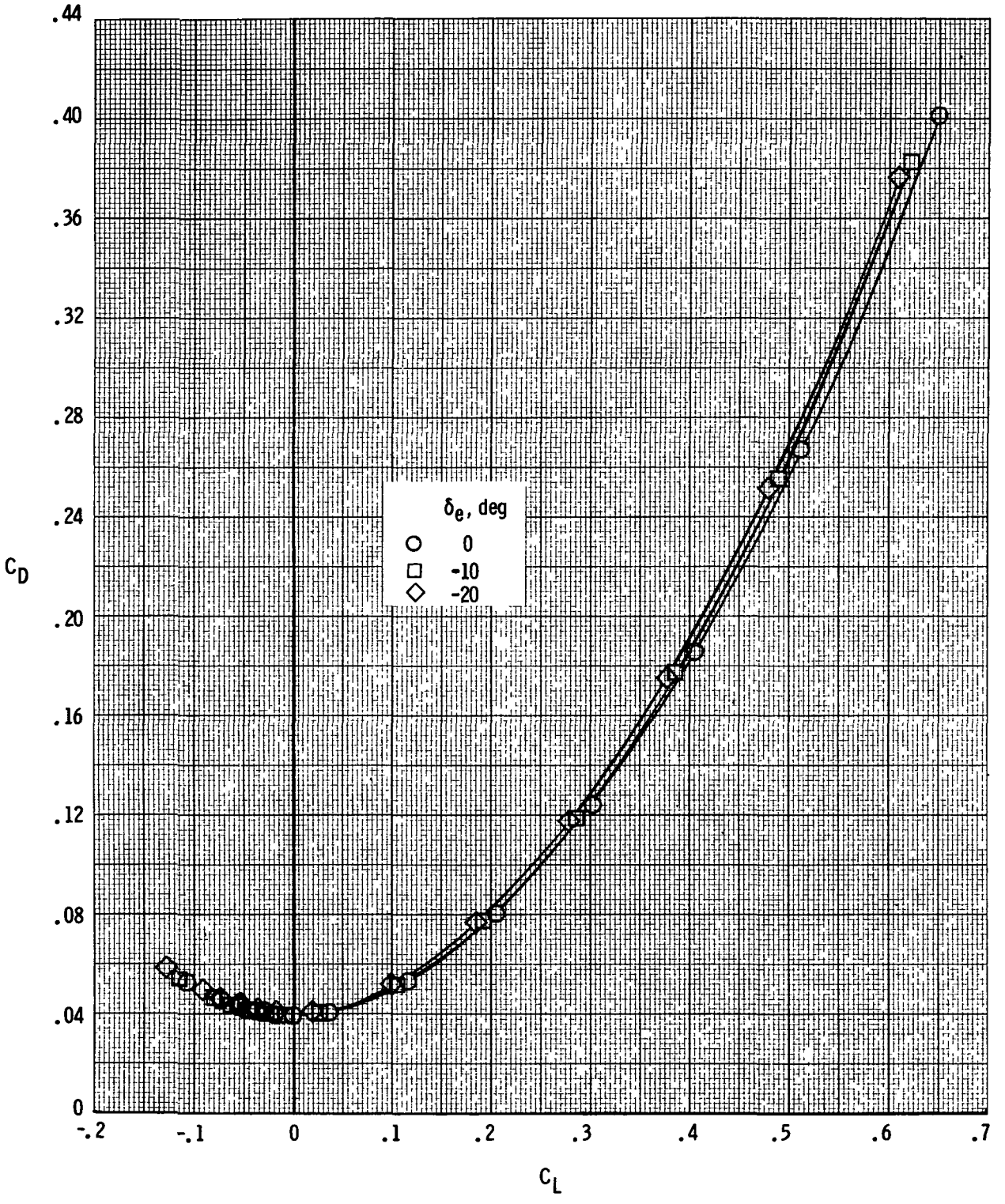

(c) C_D as a function of C_L. M = 3.95.

Figure 9.- Continued.

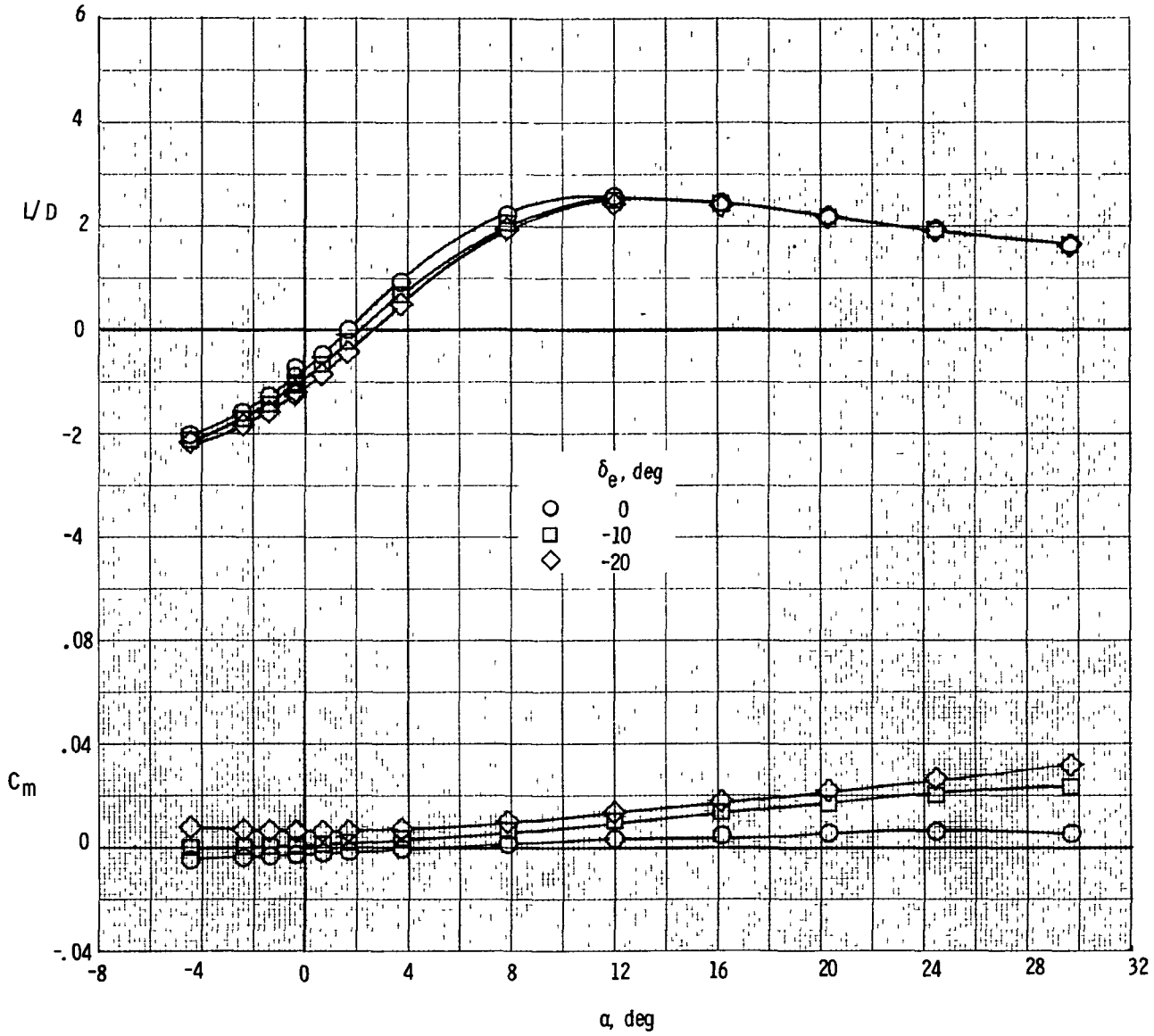

(d) C_m and L/D as functions of α. M = 3.95.

Figure 9.- Continued.

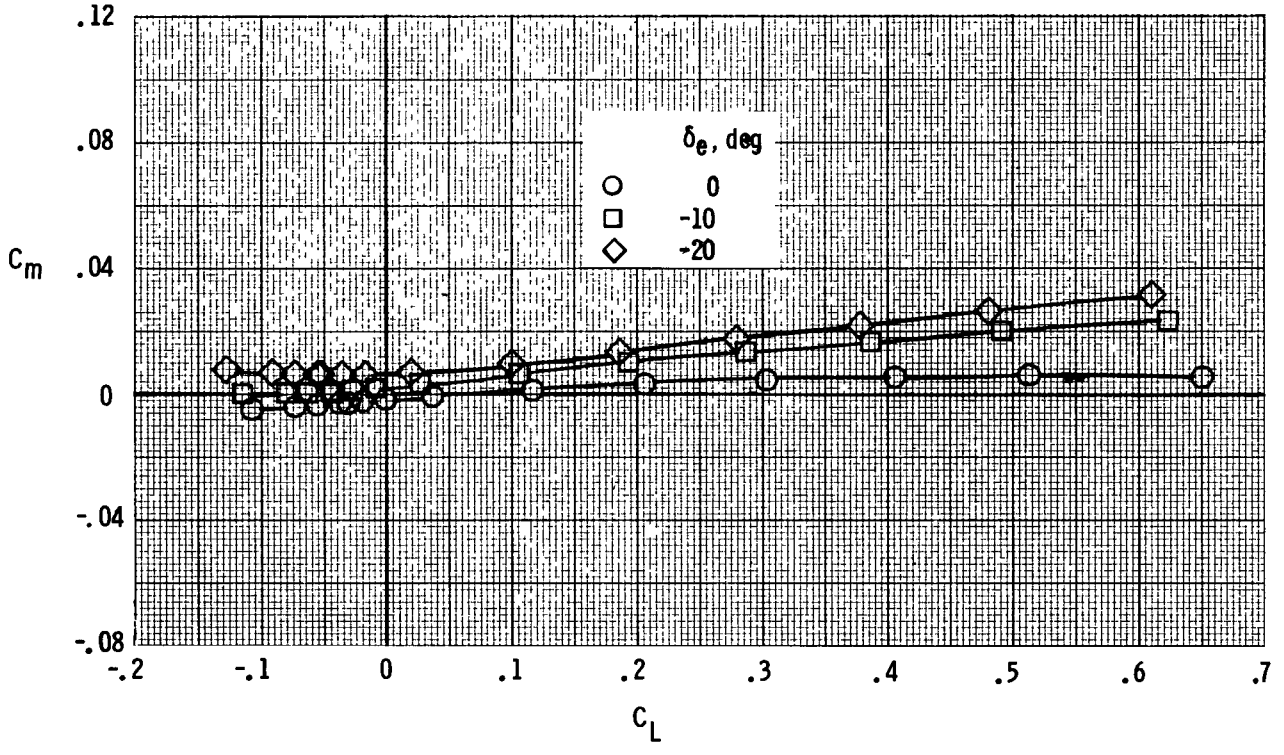

(e) C_m as a function of C_L. M = 3.95.

Figure 9.- Concluded.

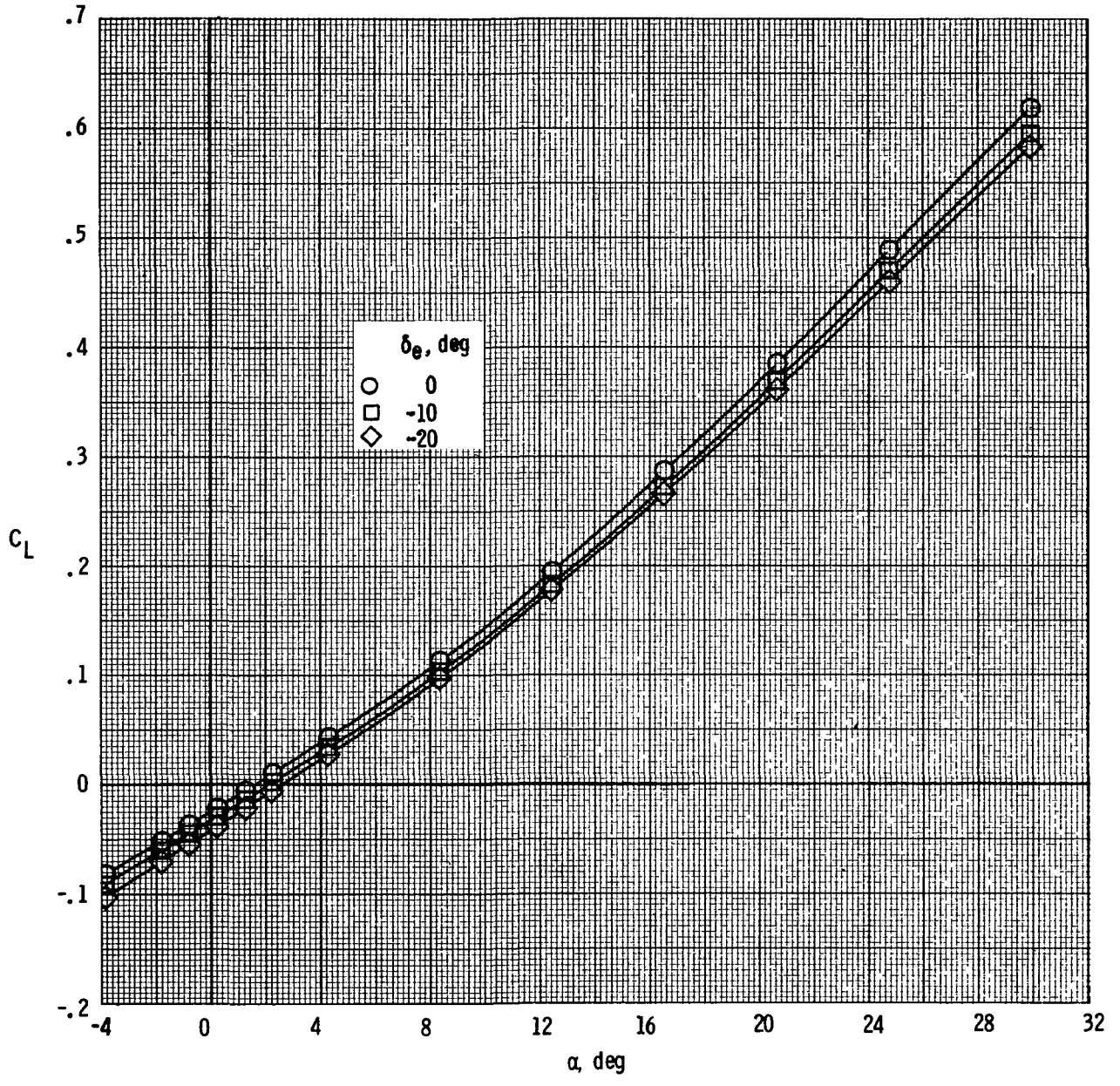

(a) C_L as a function of α. M = 4.63.

Figure 10.- Static longitudinal stability and trim characteristics at M = 4.63.

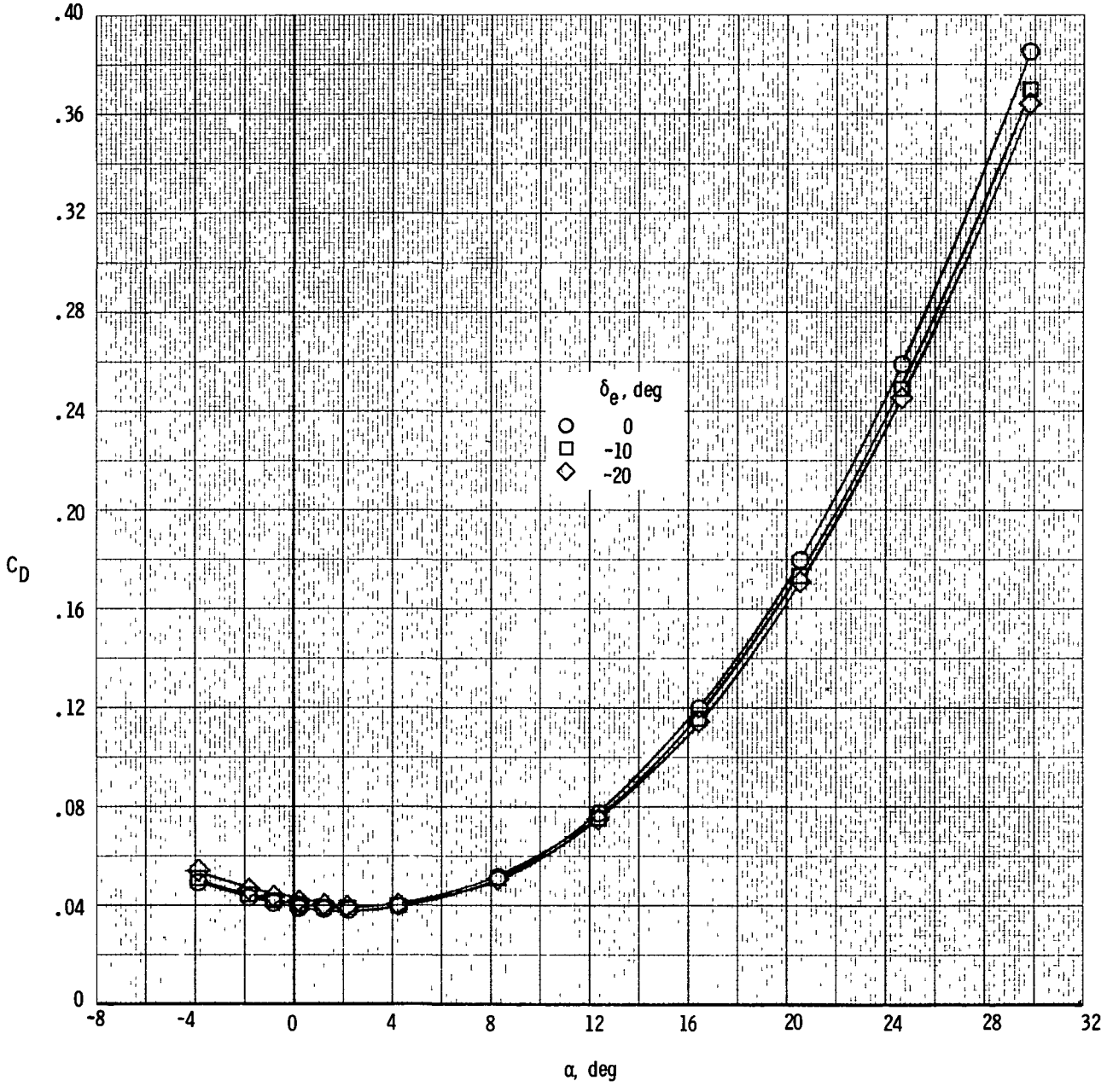

(b) C_D as a function of α. M = 4.63.

Figure 10.- Continued.

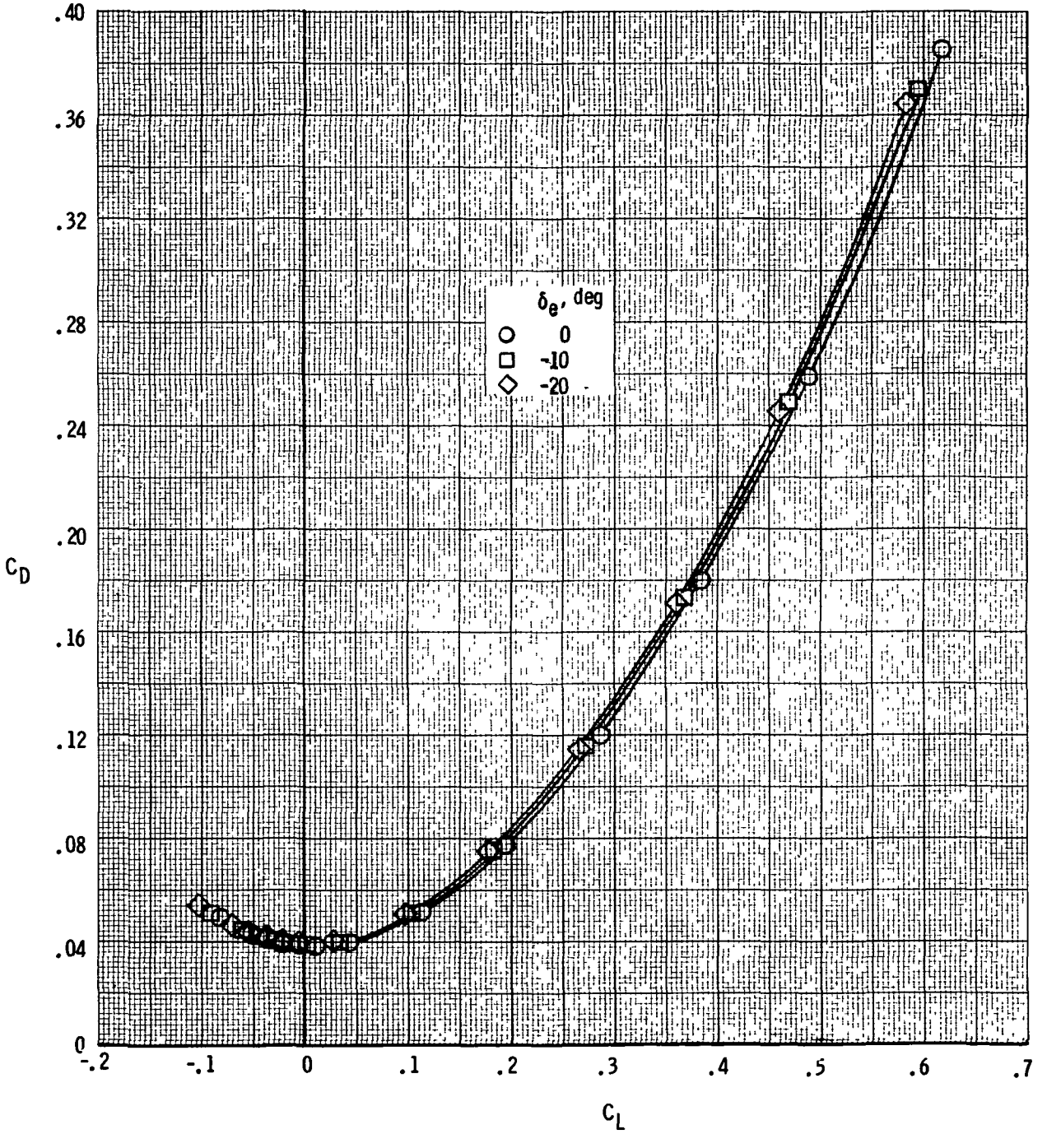

(c) C_D as a function of C_L. M = 4.63.

Figure 10.- Continued.

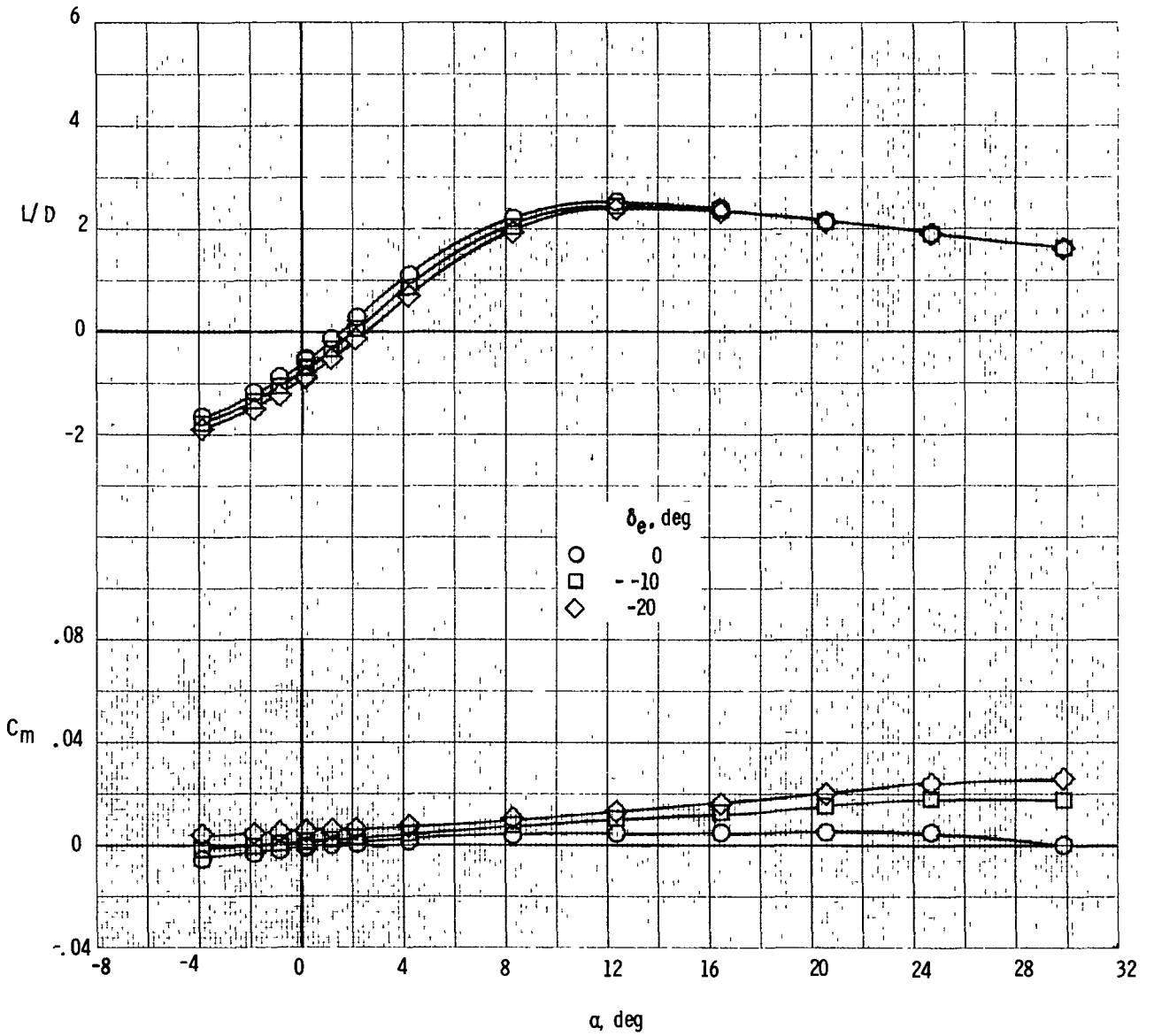

(d) C_m and L/D as functions of α. M = 4.63.

Figure 10.- Continued.

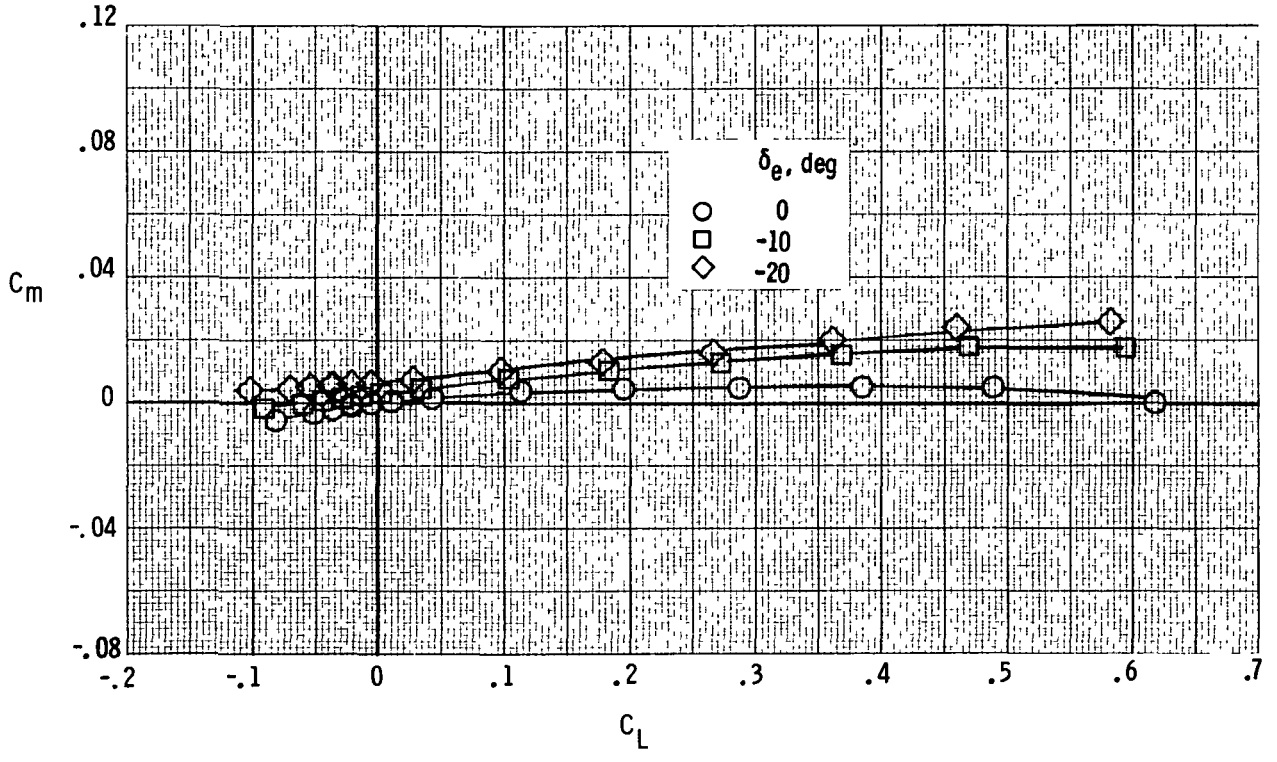

(e) C_m as a function of C_L. M = 4.63.

Figure 10.- Concluded.

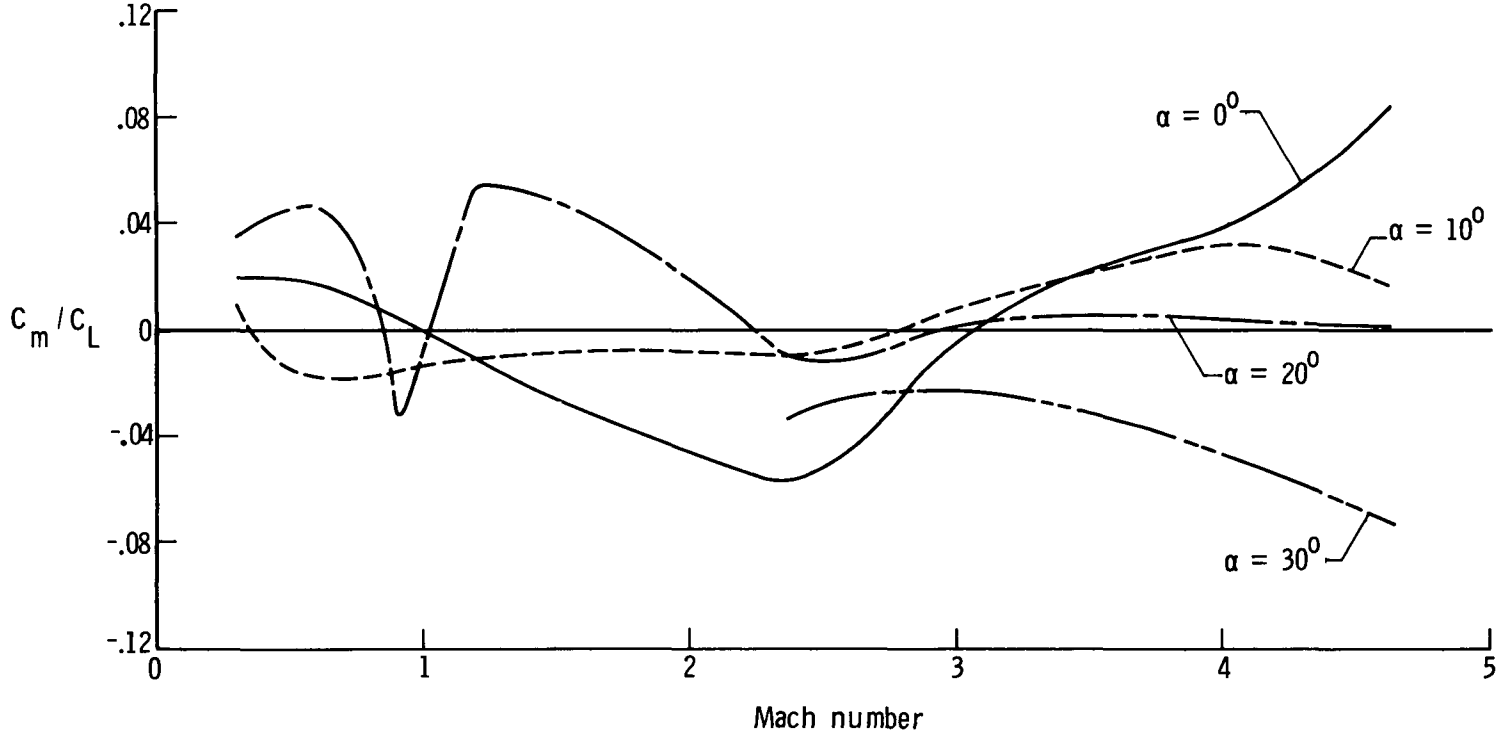

(a) C_m/C_L as a function of M.

Figure 11.- Summary of longitudinal characteristics. $\delta_e = 0^o$.

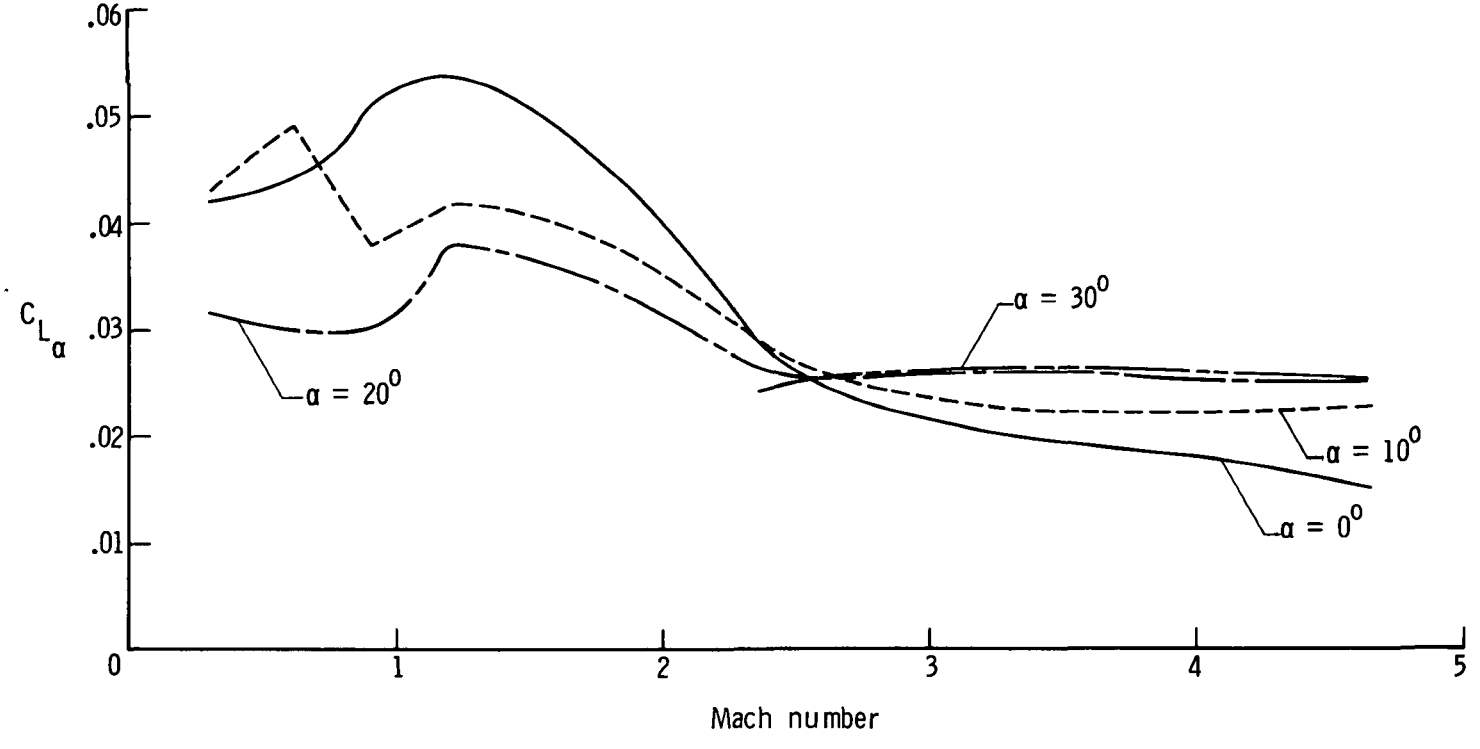

(b) C_{L_α} as a function of M.

Figure 11.- Concluded.

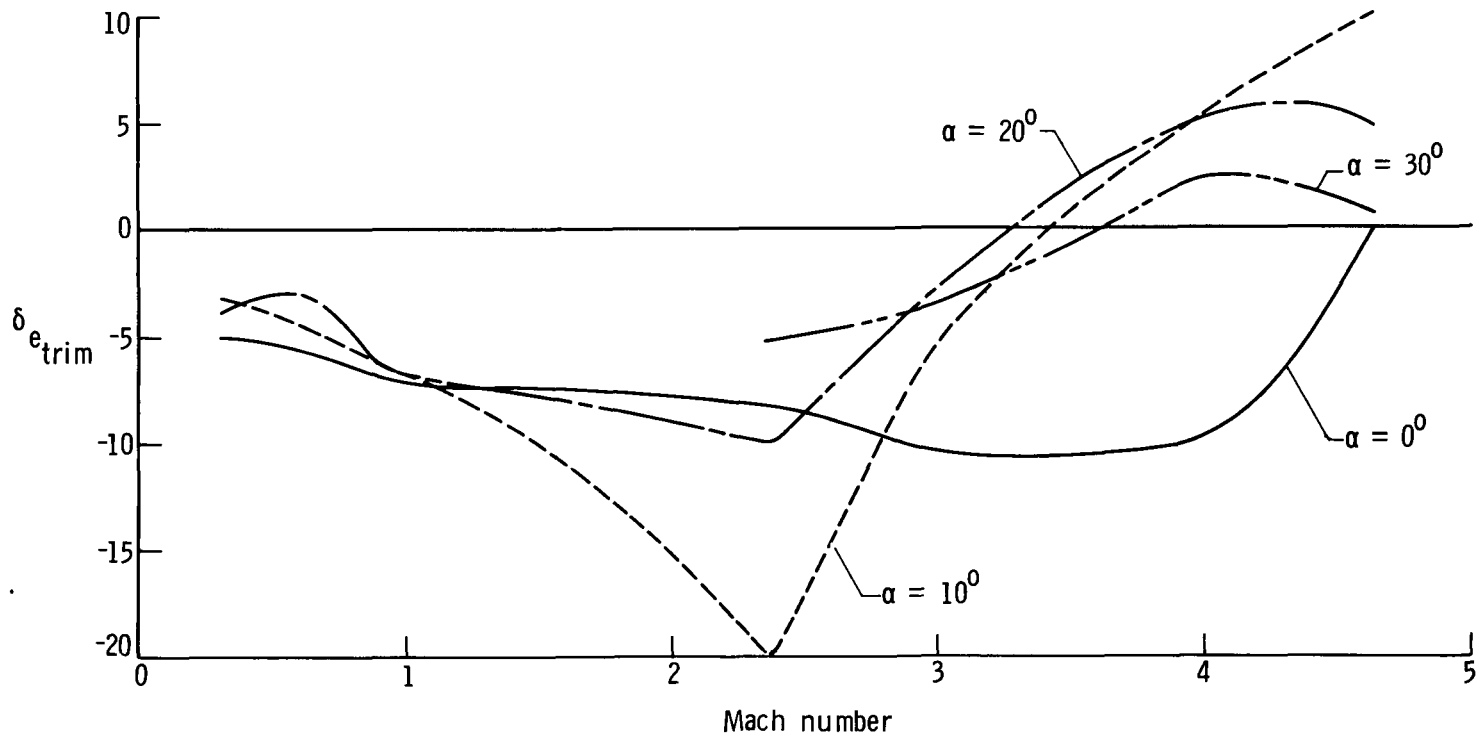

(a) $\delta_{e_{trim}}$ as a function of M.

Figure 12.- Summary of longitudinal trim characteristics.

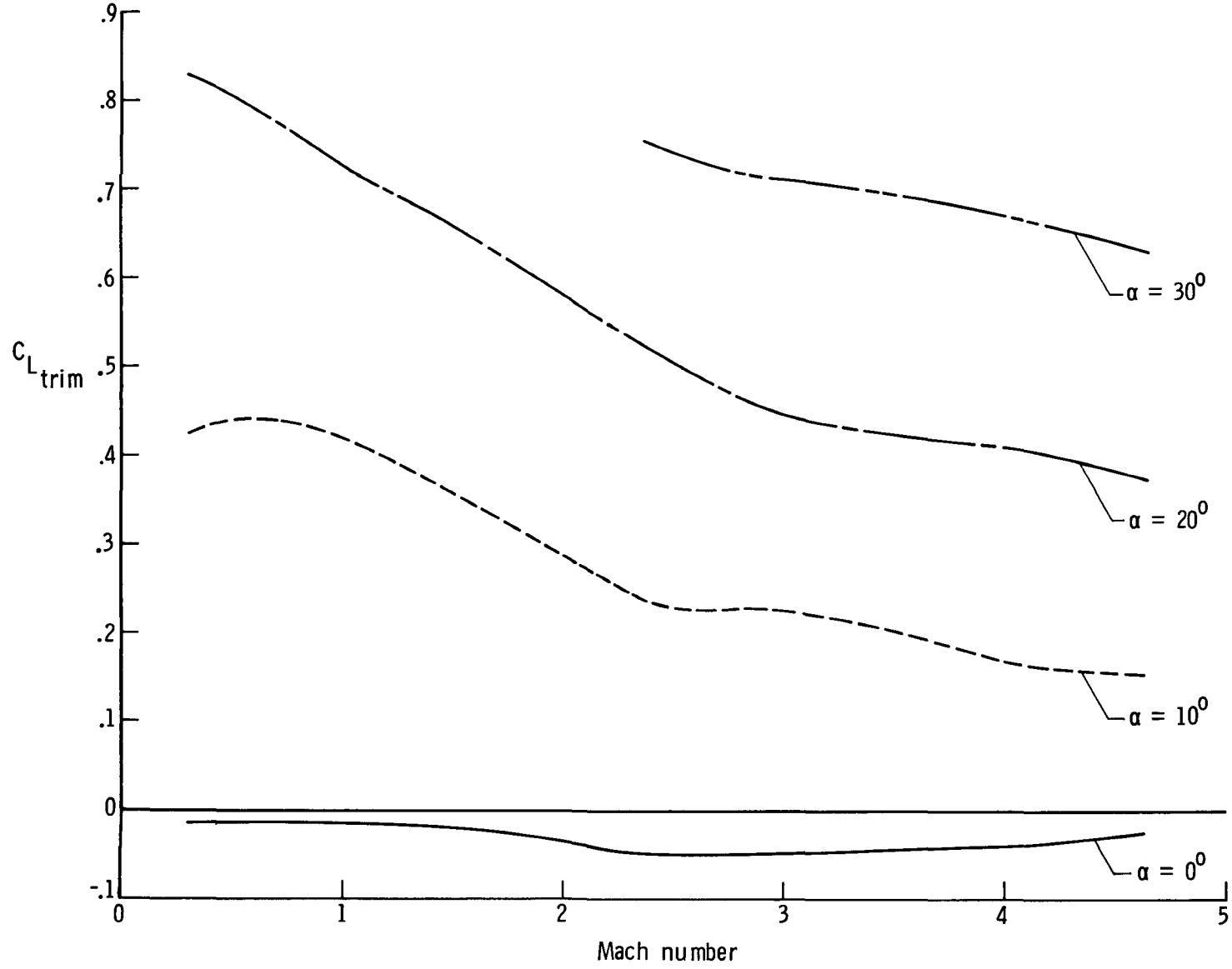

(b) $C_{L_{trim}}$ as a function of M.

Figure 12.- Continued.

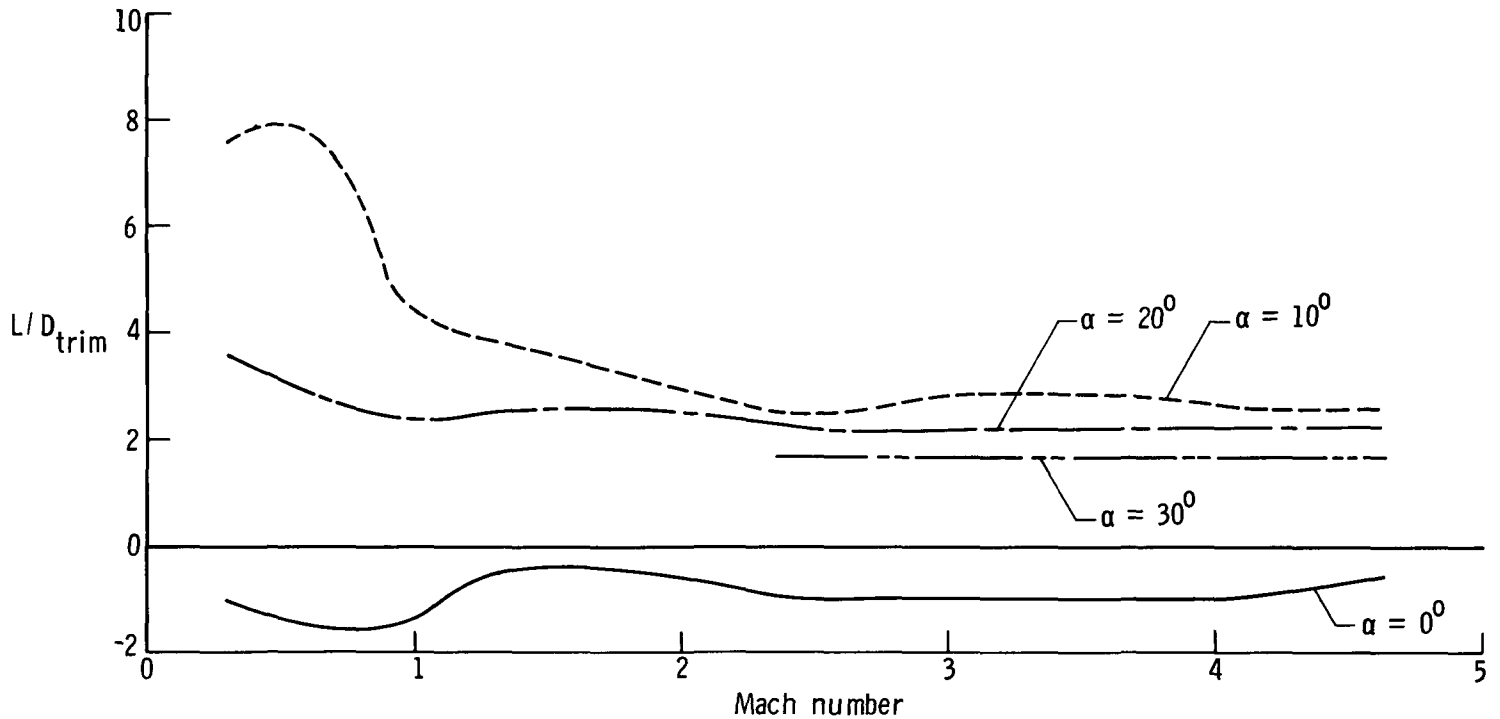

(c) L/D_{trim} as a function of M.

Figure 12.- Concluded.

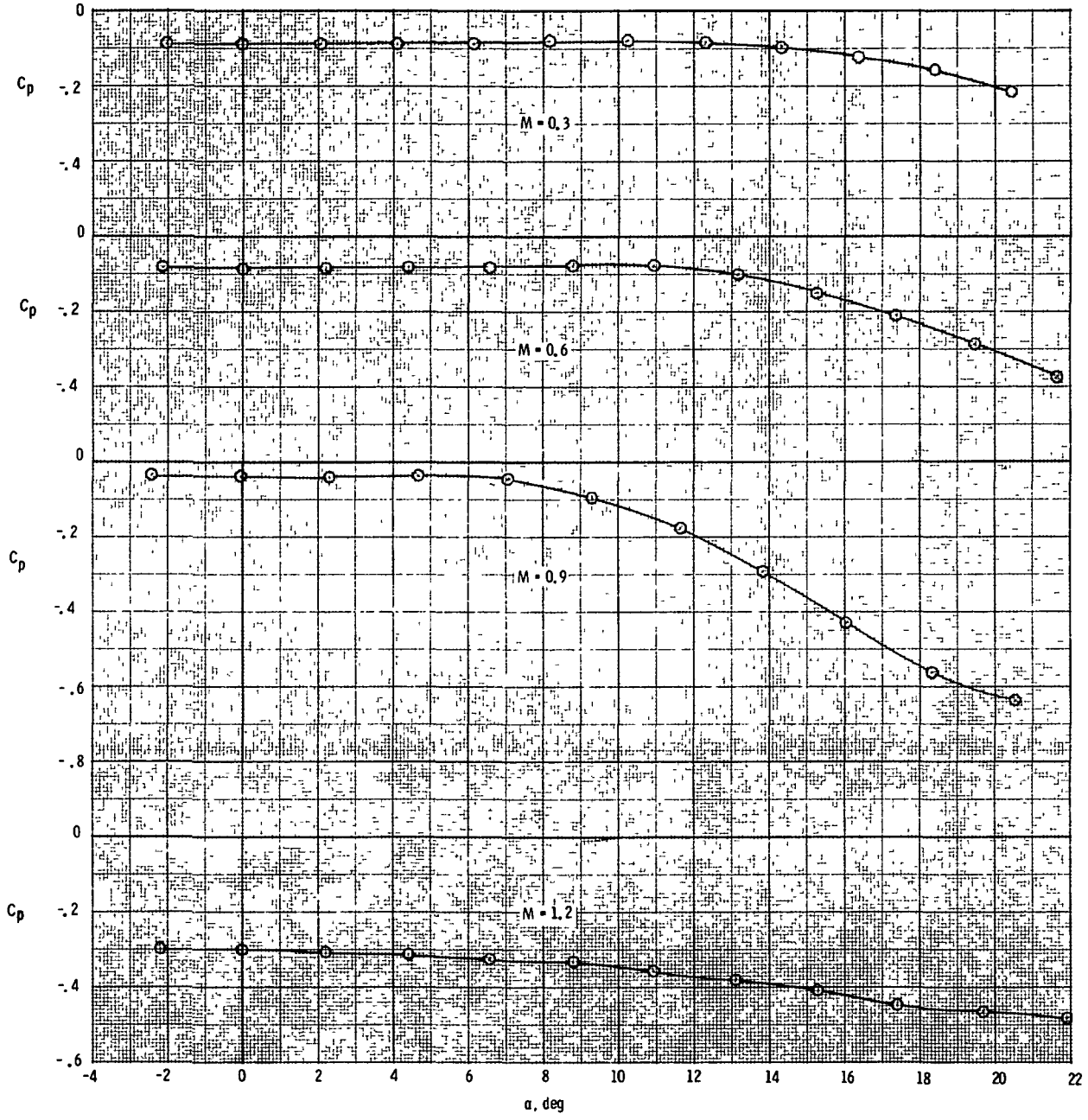

(a) M = 0.3 to 1.2.

Figure 13.- Base pressure data measured during tests.

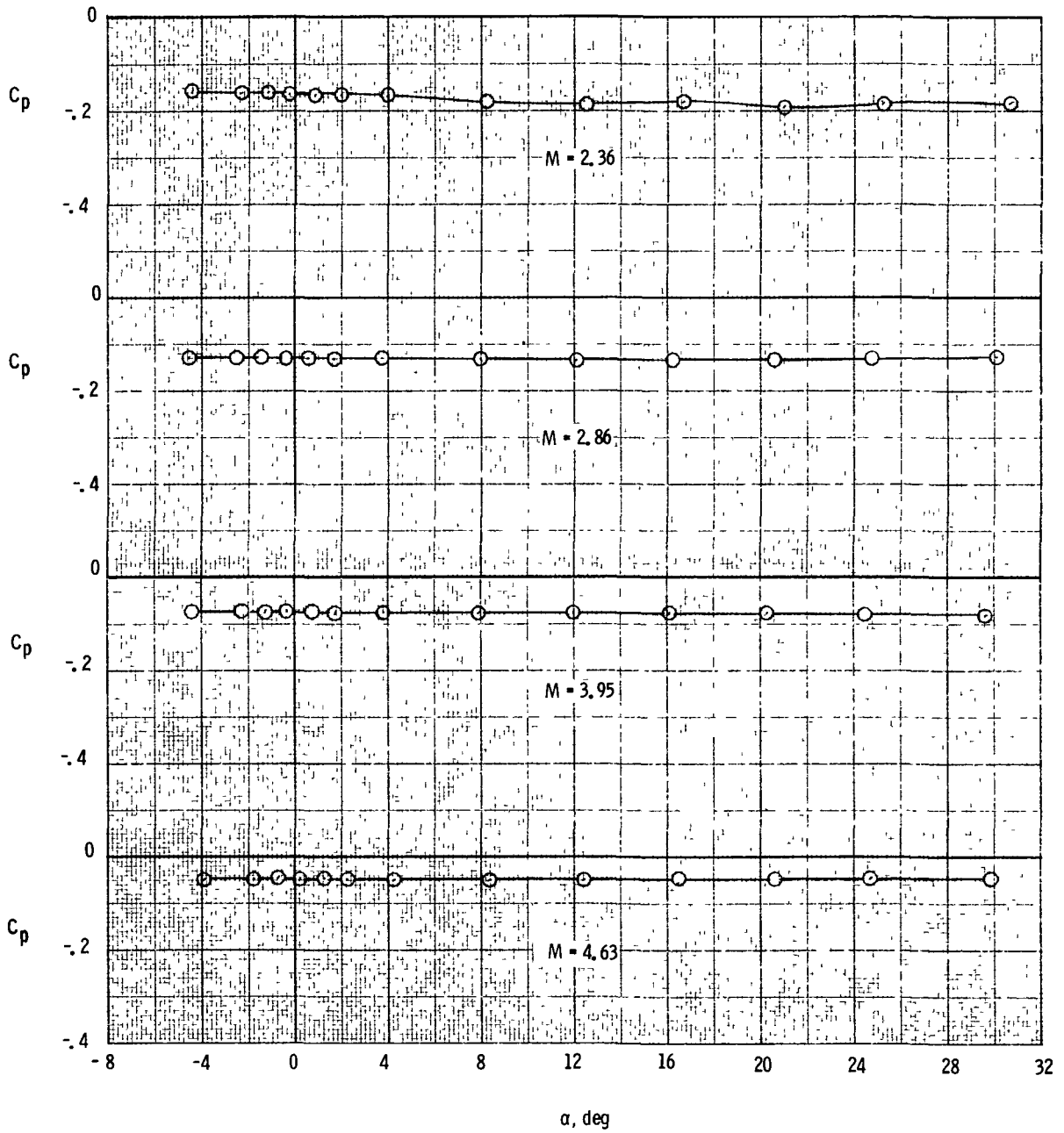

(b) M = 2.36 to 4.63.

Figure 13.- Concluded.

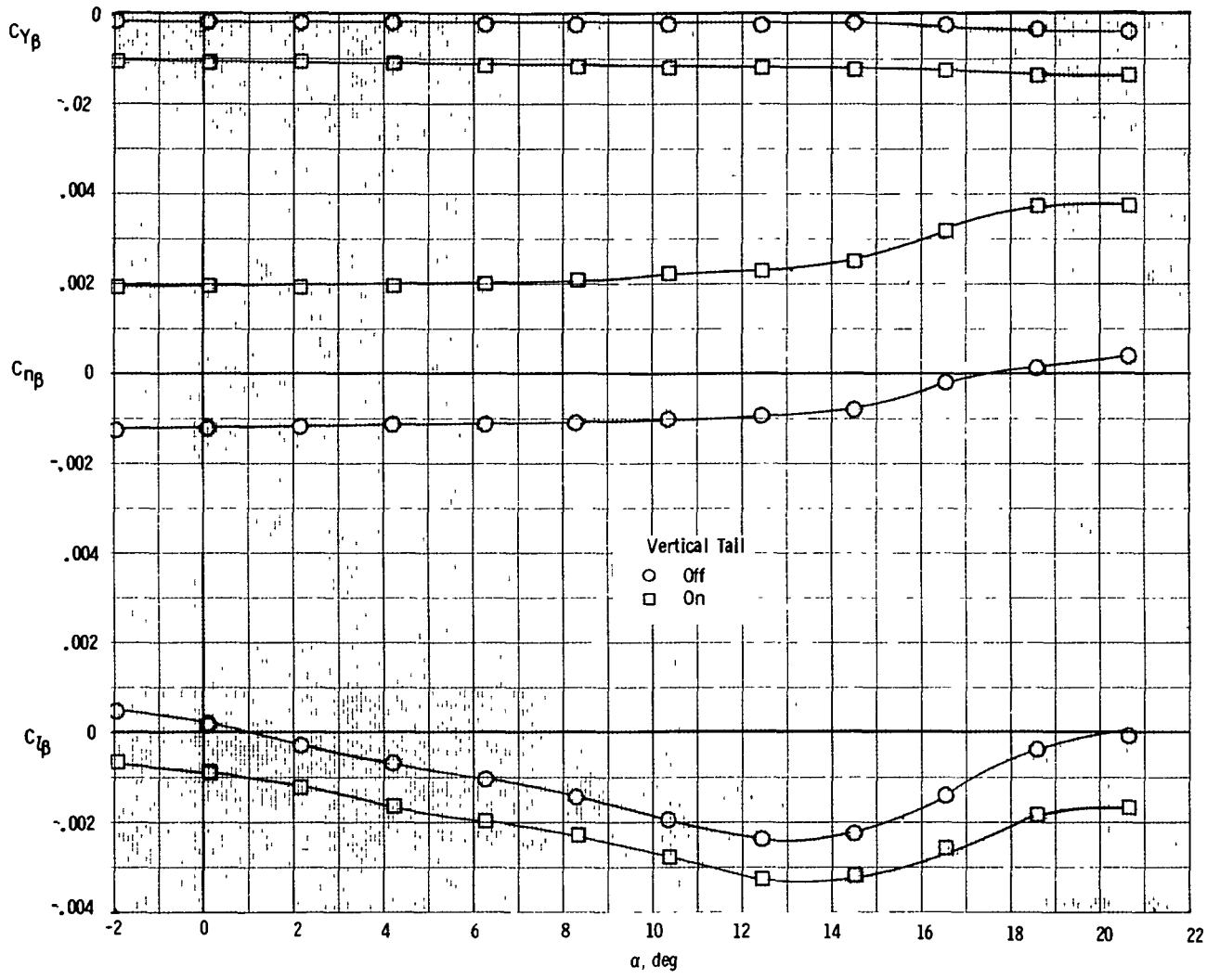

(a) M = 0.3.

Figure 14.- Static lateral-directional characteristics of model. $\delta_e = 0$, $\delta_r = 0$.

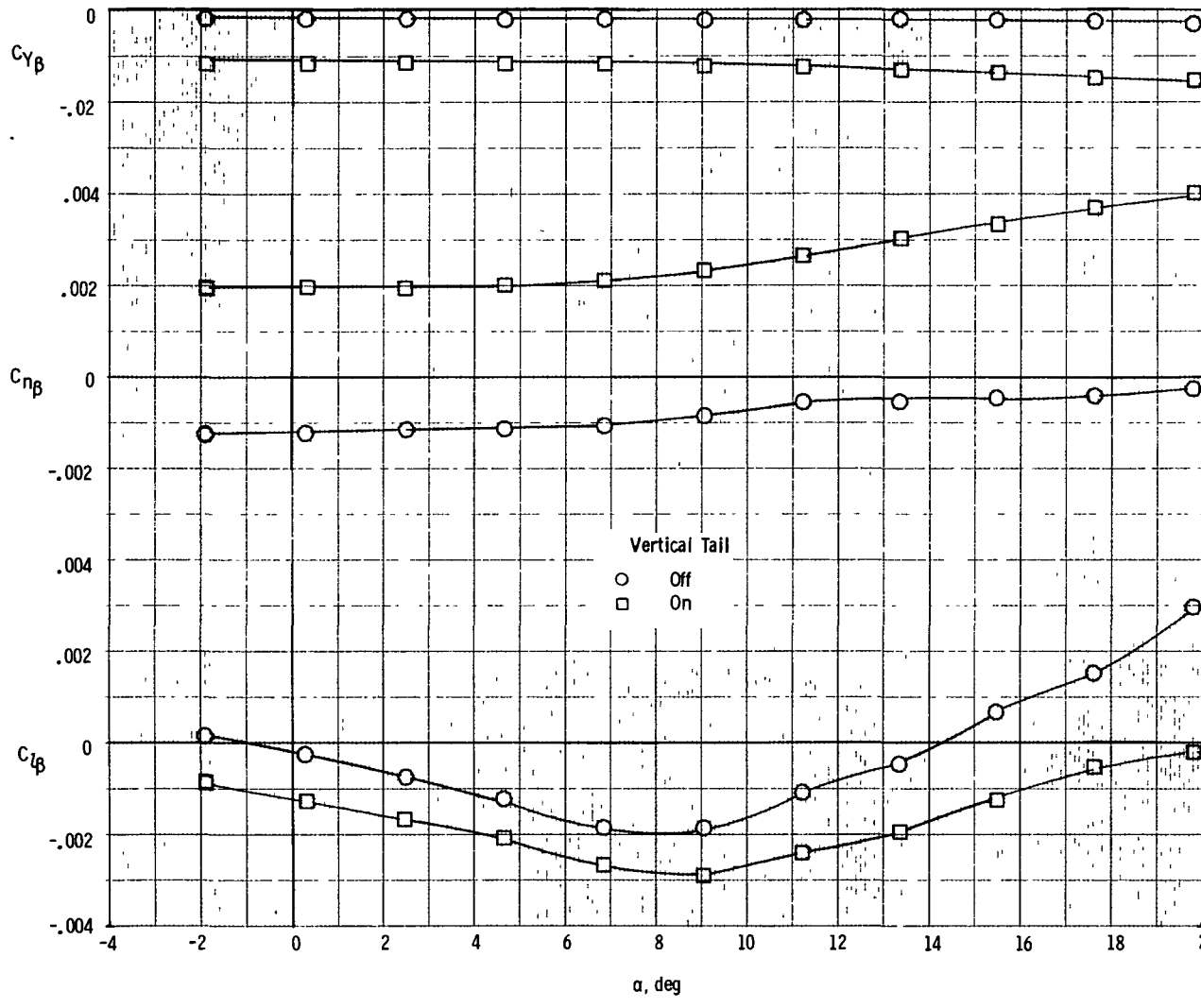

(b) M = 0.6.

Figure 14.- Continued.

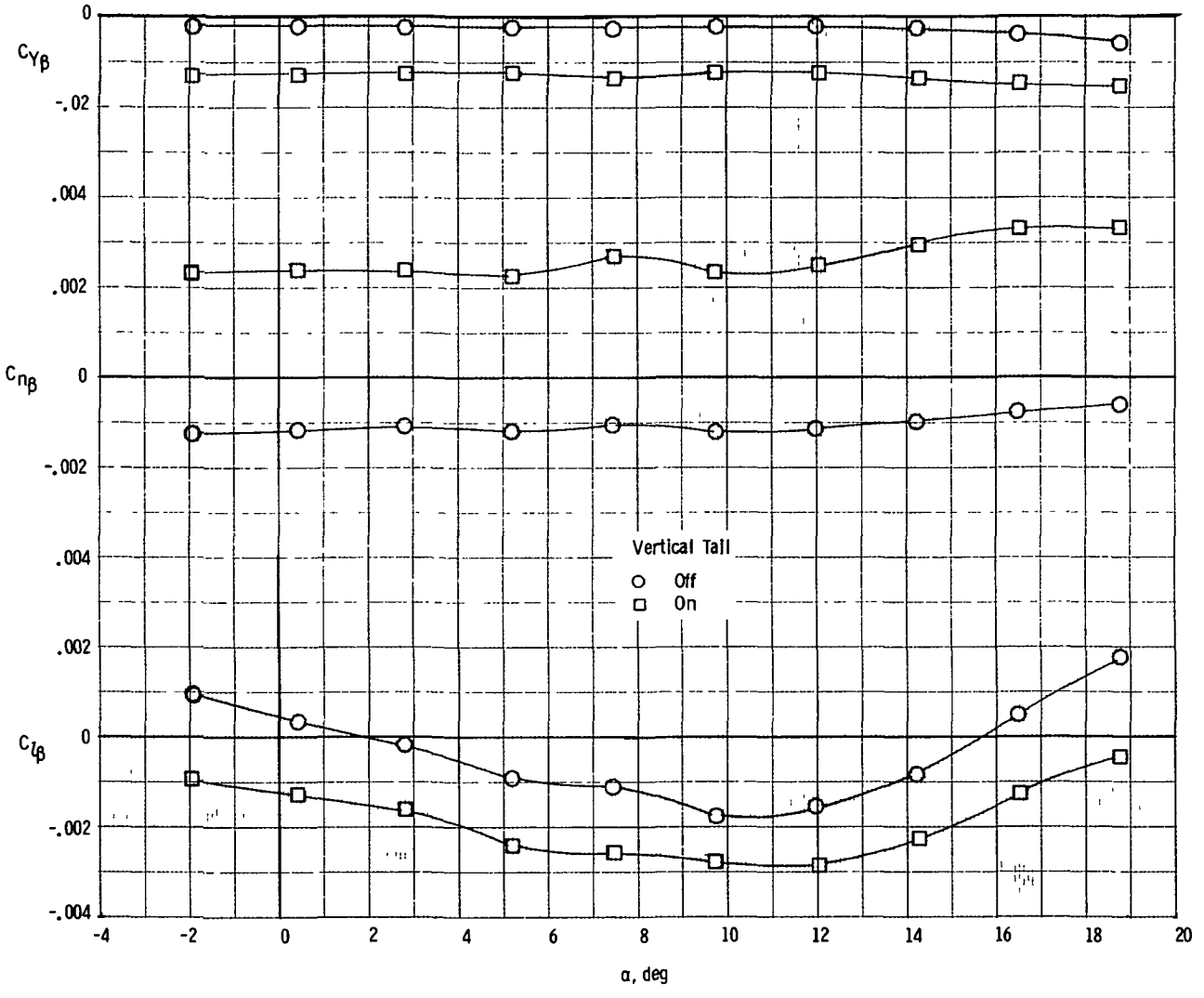

(c) M = 0.9.

Figure 14.- Continued.

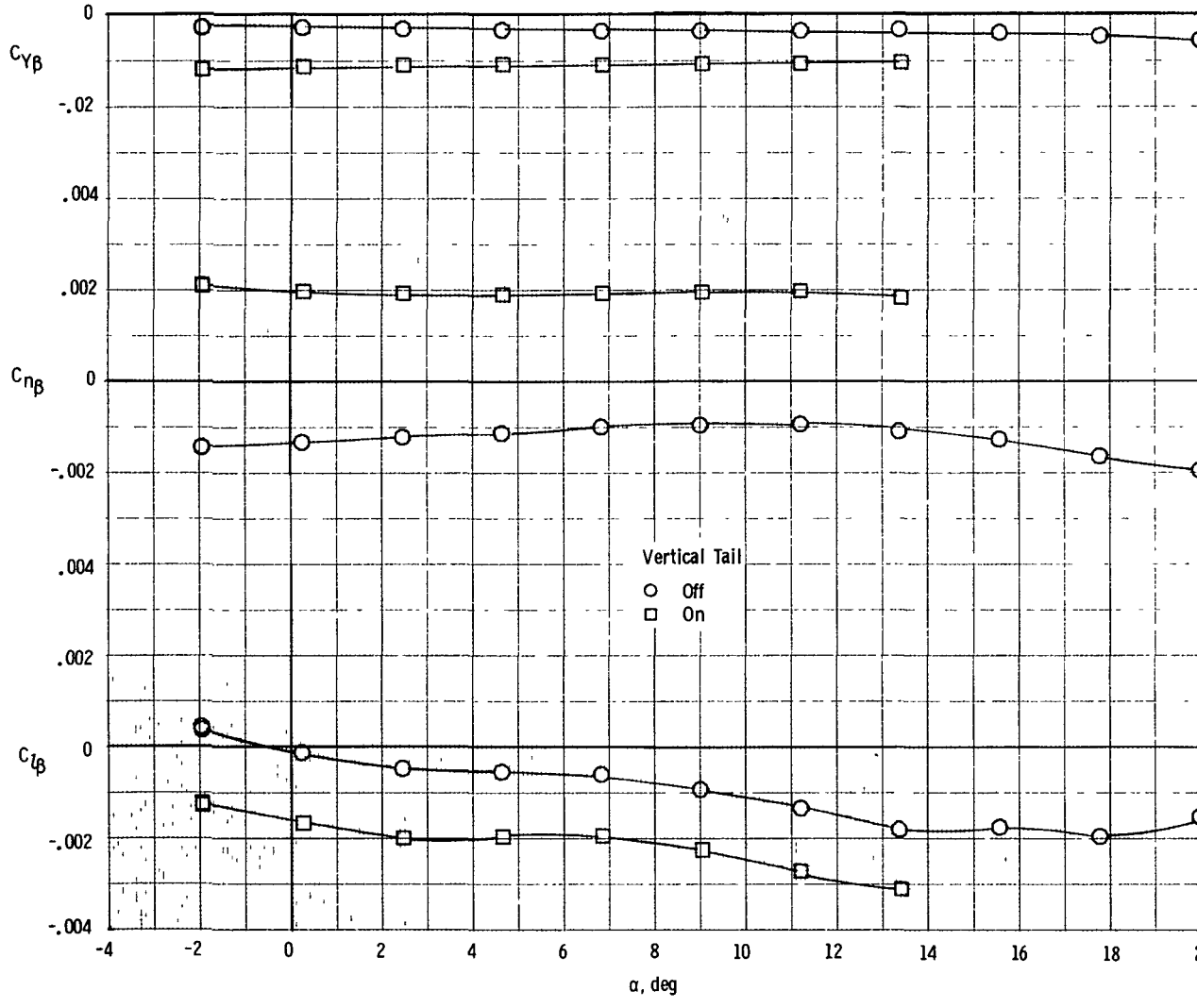

(d) M = 1.2.

Figure 14.- Continued.

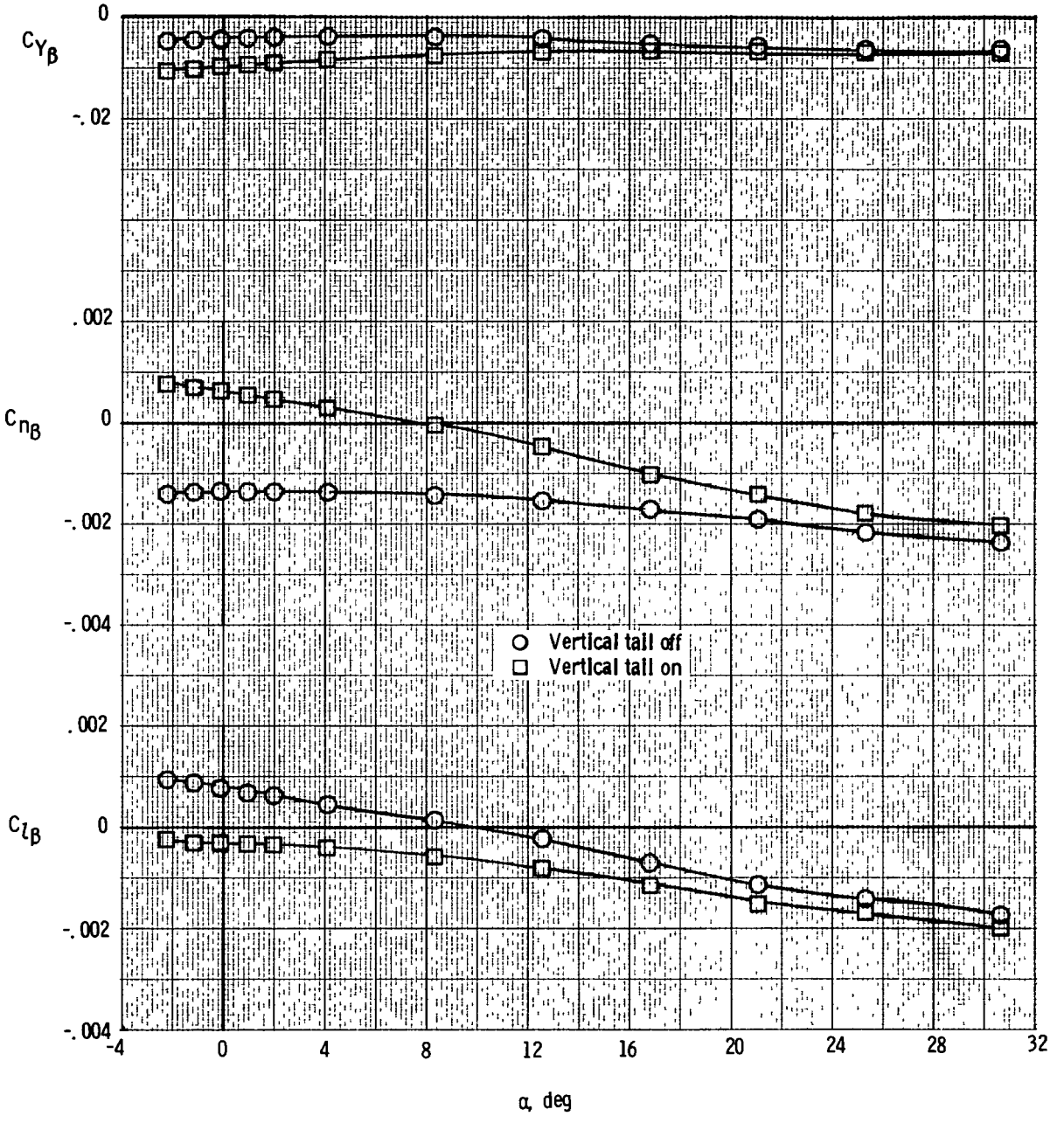

(e) M = 2.36.

Figure 14.- Continued.

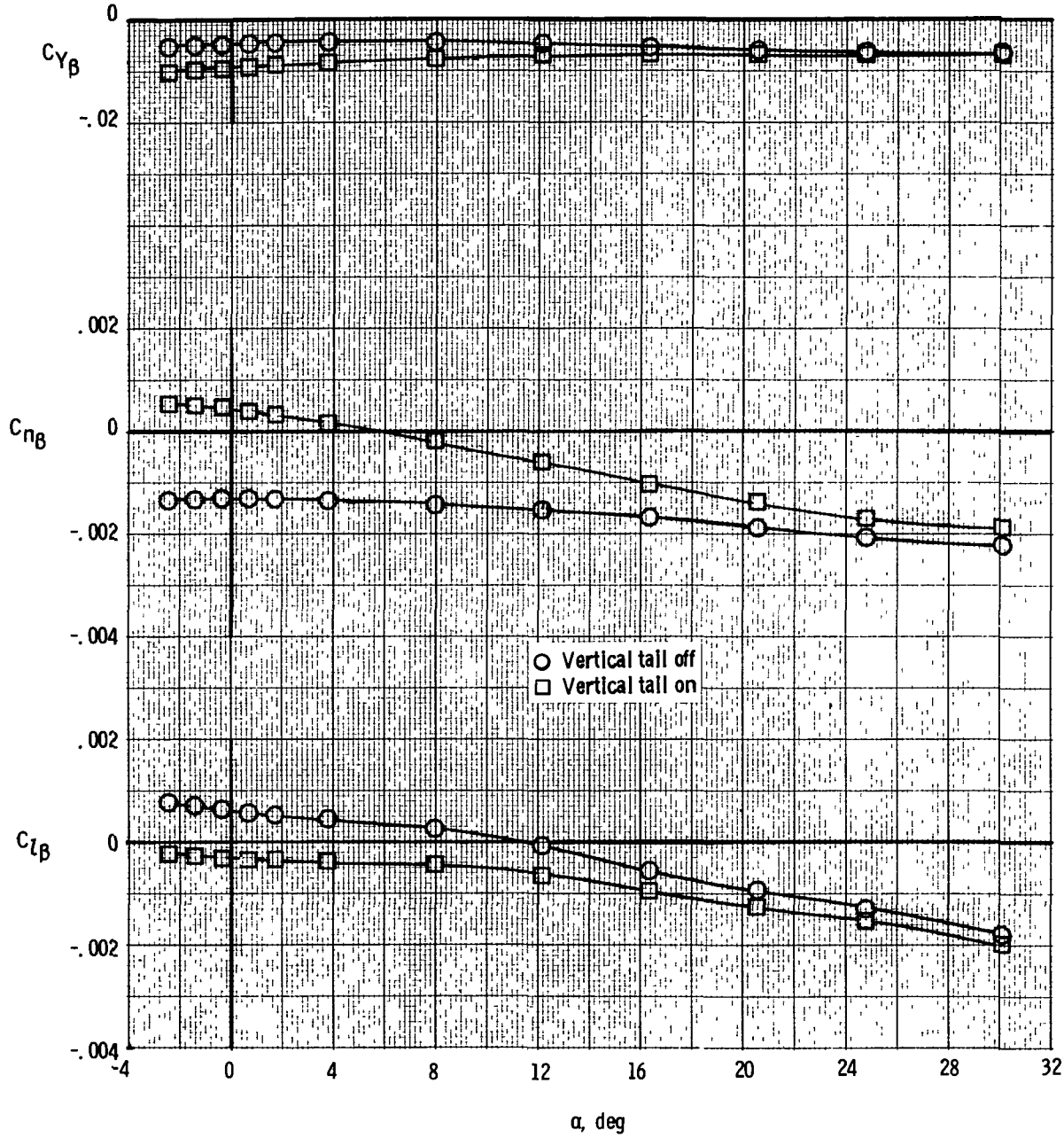

(f) M = 2.86.

Figure 14.- Continued.

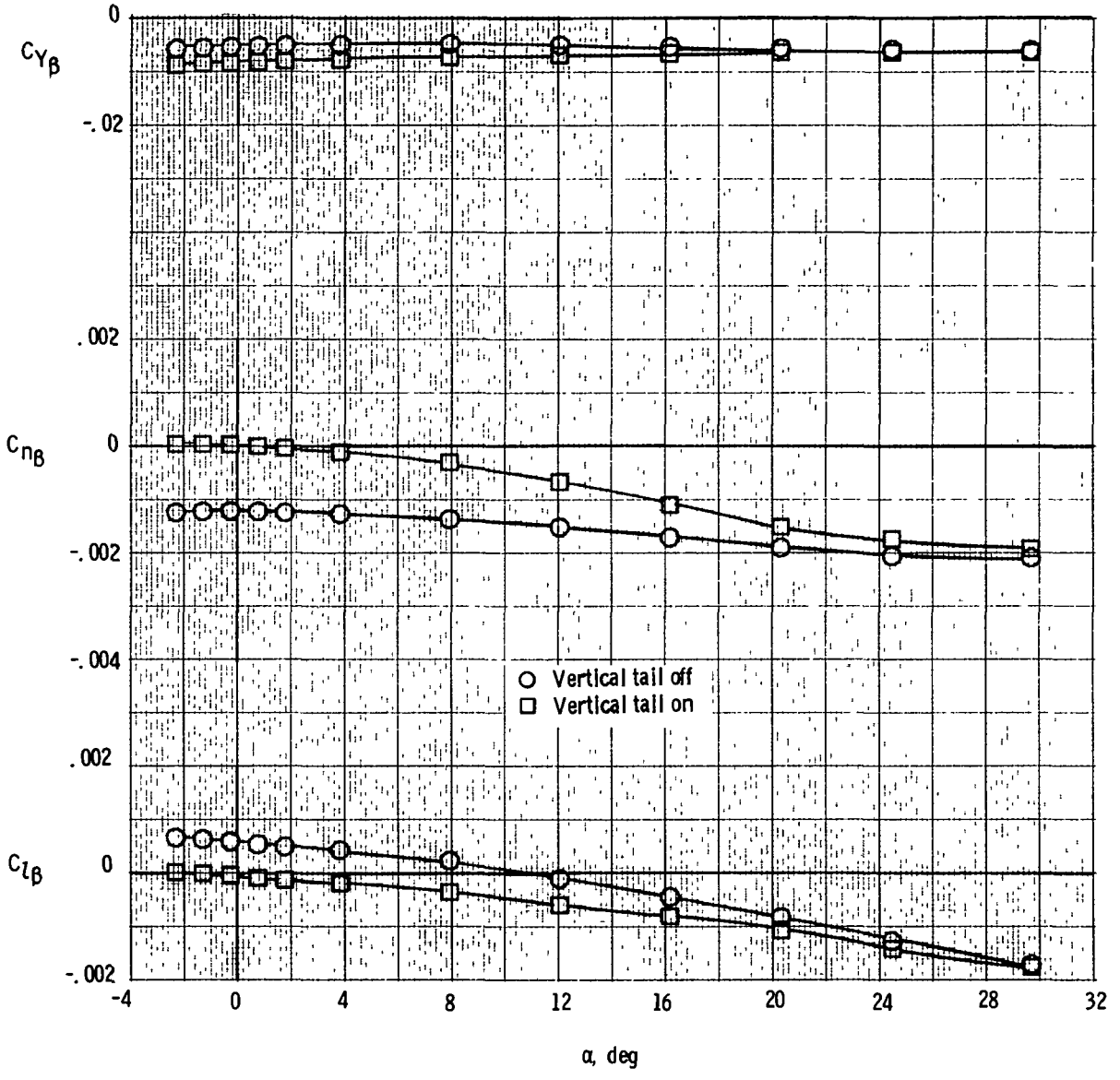

(g) M = 3.95.

Figure 14.- Continued.

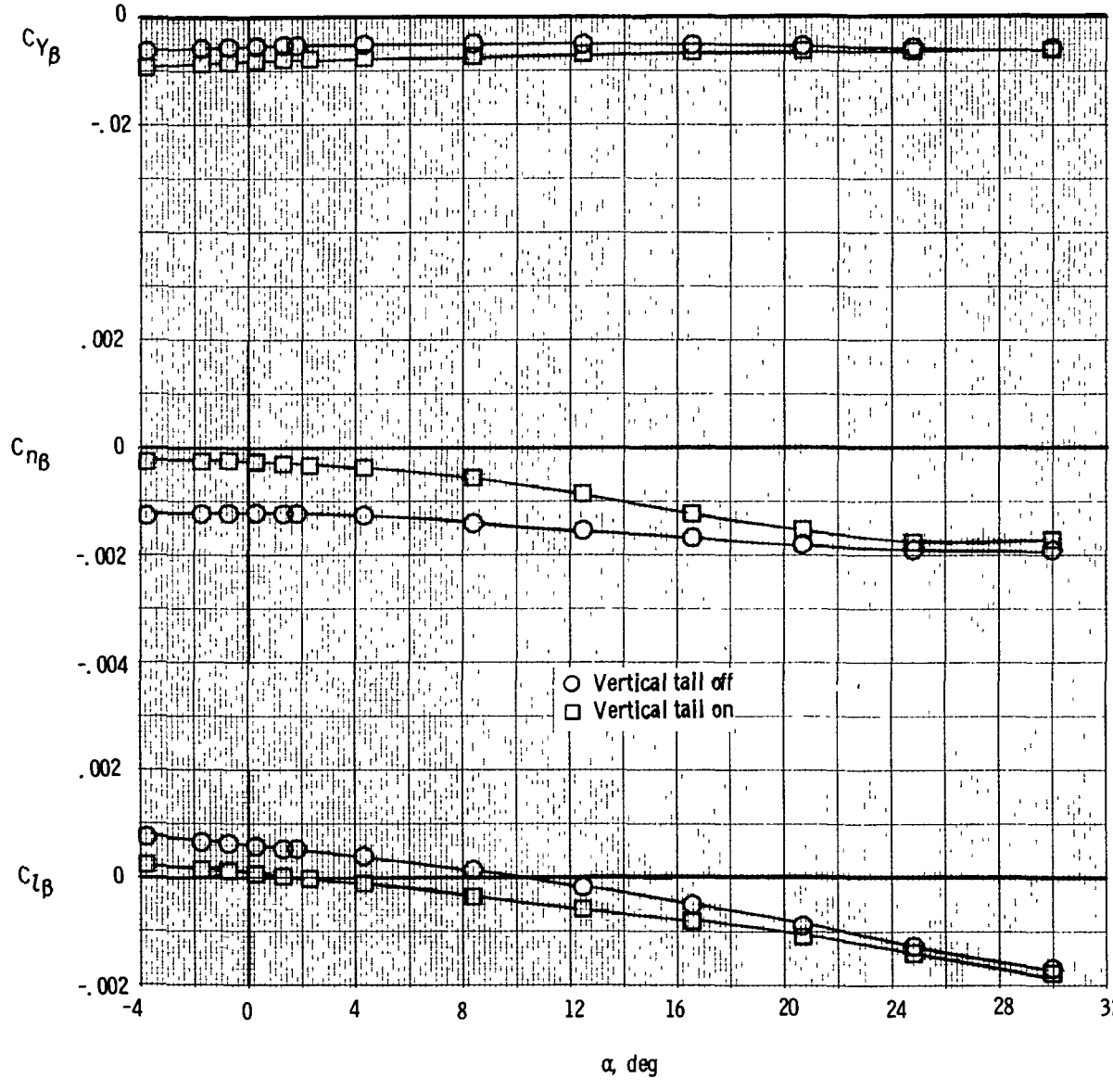

(h) M = 4.63.

Figure 14.- Concluded.

1 Report No	2 Government Accession No	3 Recipient's Catalog No
NASA TM-74056		

4 Title and Subtitle	5 Report Date
STATIC AERODYNAMIC CHARACTERISTICS OF A SINGLE-STAGE-TO-ORBIT VEHICLE WITH LOW PLANFORM LOADING AT MACH NUMBERS FROM 0.3 TO 4.63	November 1977
	6 Performing Organization Code

7 Author(s)	8 Performing Organization Report No
Delma C. Freeman, Jr., and Roger H. Fournier	L-11797
	10 Work Unit No
	506-26-10-08

9 Performing Organization Name and Address	11 Contract or Grant No
NASA Langley Research Center Hampton, VA 23665	
	13 Type of Report and Period Covered
	Technical Memorandum

12 Sponsoring Agency Name and Address	14 Sponsoring Agency Code
National Aeronautics and Space Administration Washington, DC 20546	

15 Supplementary Notes

16 Abstract

An investigation was conducted in the Langley 8-foot transonic pressure tunnel and in the Langley Unitary Plan wind tunnel to determine the longitudinal and lateral aerodynamic characteristics of a single-stage-to-orbit vehicle which utilizes an all metallic, hot structure, thermal protection system resulting in low planform loading. The model was tested over a Mach number range from 0.3 to 4.63 for angles of attack from -4° to 32° at both 0° and 5° sideslip.

17 Key Words (Suggested by Author(s))	18 Distribution Statement
Entry-vehicle aerodynamics Single-stage-to-orbit vehicle Advanced space transportation systems	Unclassified - Unlimited Subject Category 15

19 Security Classif (of this report)	20 Security Classif (of this page)	21 No of Pages	22 Price*
Unclassified	Unclassified	66	$4.50

* For sale by the National Technical Information Service, Springfield Virginia 22161

NASA-Langley, 1977

National Aeronautics and
Space Administration

Washington, D.C.
20546

Official Business
Penalty for Private Use, $300

THIRD-CLASS BULK RATE

Postage and Fees Paid
National Aeronautics and
Space Administration
NASA-451

U.S.MAIL

2 2 1U.B. 103177 S90844HU
MCDONNELL DOUGLAS CORP
ATTN: PUBLICATIONS GROUP, PR 15246
P O BOX 516
ST LOUIS MO 63166

NASA

POSTMASTER: If Undeliverable (Section 158 Postal Manual) Do Not Return